Design, Analysis and Modeling of a Modular Navy Integrated Power and Energy Corridor Cooling System

by

Wade T. Meyers

Submitted to the Department of Mechanical Engineering
in partial fulfillment of the requirements for the degrees of

MASTER OF SCIENCE IN NAVAL ARCHITECTURE AND MARINE ENGINEERING

and

MASTER OF SCIENCE IN MECHANICAL ENGINEERING

at the

MASSACHUSETTS INSTITUTE OF TECHNOLOGY

May 2024

Authored by: Wade T. Meyers
B.S., Chemical Engineering, North Carolina State University (2012)
May 2024

Certified by: Julie C. Chalfant
Research Scientist, Thesis Supervisor

Certified by: Michael Triantafyllou
Professor of Mechanical and Ocean Engineering, Thesis Supervisor

Accepted by: Nicolas Hadjiconstantinou
Chairman
Department Committee on Graduate Theses

Design, Analysis and Modeling of a Modular Navy Integrated Power and Energy Corridor Cooling System

by

Wade T. Meyers

Submitted to the Department of Mechanical Engineering
on May 2024 in partial fulfillment of the requirements for the degrees of

MASTER OF SCIENCE IN NAVAL ARCHITECTURE AND MARINE ENGINEERING

and

MASTER OF SCIENCE IN MECHANICAL ENGINEERING

ABSTRACT

In response to the escalating demand for electricity onboard future naval vessels, the Design Laboratory of the Massachusetts Institute of Technology (MIT) Sea Grant Program, as part of a U.S. Navy research consortium for next-generation all-electric warships, is pioneering the development of the Navy Integrated Power and Energy Corridor (NiPEC). This innovative system is designed to enhance the power distribution capabilities of warships like the forthcoming DDG(X), which is expected to require significant electrical power to support advanced offensive and defensive systems. NiPEC features a network of modular compartments that independently or collectively perform energy storage, conversion, protection, control, isolation, and transfer functions. Central to this system is the integrated Power Electronics Building Block (iPEBB), a self-contained, power-dense converter tailored to manage the ships' stochastic and dynamic loads efficiently. However, realizing the full potential of iPEBB's advanced semiconductor technology presents significant challenges, particularly in thermal management. This aspect is further complicated by the constraints imposed by indirect liquid cooling methods and the necessity for sailor-friendly design considerations. Preliminary analyses by Padilla et al. on heat dissipation strategies, as well as Reyes' and Chaterjee's subsequent design proposal for a NiPEC liquid cooling system highlight the operational and maintenance challenges in cooling the system's numerous components.

This thesis presents a comprehensive approach to designing a modular, compact, and indirect liquid cooling system for the NiPEC to be deployed across future all-electric Navy destroyer warships. Leveraging a combination of first-principles thermodynamic analysis, multi-physics-based modeling, and numerical analysis, the study builds upon Reyes' and Chaterjee's preliminary design to propose enhanced cooling system architectures that meet stringent military standards while ensuring robust thermal management. Further, the design and detailed analysis of this compact heat exchanger significantly contribute to enabling the modular construction of the NiPEC cooling system alongside the concurrent assembly of the NiPEC electrical system. This investigation also delves into the extraction and application of response surface models that elucidate the dynamic interdependencies among various response variables—such as the overall heat transfer coefficient and heat transfer rates—arising from changes in explanatory variables like inlet velocities, temperatures, and

the specific geometry of the heat exchanger. This multifaceted analysis not only refines the cooling system's efficiency but also aligns it with the modular integration requirements of military naval applications.

Thesis supervisor: Julie C. Chalfant
Title: Research Scientist

Thesis supervisor: Michael Triantafyllou
Title: Professor of Mechanical and Ocean Engineering

Acknowledgments

I would like to express my deepest gratitude to my thesis supervisors, Dr. Julie Chalfant and Professor Michael Triantafyllou, for their invaluable guidance, feedback, and encouragement throughout this year-long endeavor. Their comprehensive knowledge in various fields of study, coupled with the resources and support they provided, enabled me to navigate the challenging aspects of my research. I feel remarkably fortunate to have had the opportunity to learn from their expertise and to have gained the confidence to tackle critical points of my study under their direction.

I would also like to extend my thanks to Joe Grippe and Steve Wilgrigs from the Naval Surface Warfare Center Philadelphia Division, as well as David Underwood and Geoff Campbell from Micro Cooling Solutions. Their expertise and guidance into current and future U.S. Navy cooling system architectures were invaluable, and they provided crucial references and insights on how my design could be integrated within this context.

I wish to express my gratitude for the contributions and sponsorship of Kelly Cooper and CAPT L.J. Petersen, USN (Ret.) from the U.S. Office of Naval Research (ONR). This material is based upon research supported by the U.S. Office of Naval Research under award number ONR N00014-21-1-2124 Electric Ship Research and Development Consortium; and by the National Oceanic and Atmospheric Administration (NOAA) under Grant Number NA22OAR4170126-MIT Sea Grant College Program.

I am also sincerely grateful to Avito Lourenco, who provided me with significant assistance and guidance through the complexities of the CAD program SolidWorks. This thesis could not have been accomplished without his invaluable support.

Lastly, I extend my deepest and most heartfelt thanks to my family—my mother, brother, sister, and especially my wife. Their unwavering support, encouragement, and understanding throughout my two years at M.I.T. have been the pillars of my strength. Their belief in me instilled the confidence to persevere and successfully complete this journey. I cherish and love you all immensely.

Contents

List of Figures

List of Tables

Chapter 1

Introduction

1.1 Background

Over the past two decades, the U.S. Navy has been actively exploring the use of all-electric technologies to power its ships as it prepares for a revolution in how warfare at sea is conducted. This revolution will take the form of not only high-power pulsed mission systems and advances in kinetic energy weapons such as lasers and electromagnetic railguns, but also how warfighter vessels are propelled through the water. Future naval power distribution systems are set to function at significantly higher power levels and voltages compared to the current generation of warships. Present-day warships generally operate within a power range of 4 to 6 Megawatts (MW), utilizing 450 Volts (V) of Alternating Current (AC). In contrast, future ships are expected to operate at substantially elevated power levels near 100 MW, with voltage levels ranging from 1 kiloVolt (kV) to as high as 12 kV utilizing Direct Current (DC) [1]. In order to meet the future's advanced weapons, mission and propulsion systems, a substantial increase in the electric load output of ships is required.

This transition to an all-electric naval force represents unprecedented levels of system complexity. It involves the integration of a myriad of advanced electric power systems and technologies that are essential for electric propulsion, energy storage, and enable the integration of future electric weapons and sensors while ensuring system communality. Considering that future naval ships are anticipated to necessitate electric power in excess of 100 MW, vessels in development must have the ability to handle capability upgrades. As stated by prior Naval Sea Service Command (NAVSEA) 00 Vice Admiral (VADM) Moore, "One of the things that is really important for us as we build these platforms is to make sure that platforms have enough space, weight, and power so that you can modernize and adapt." Figure 1.1 depicts this trend of increased power demand for future warfighting vessels [2].

One entity that is focused on this revolutionary transition is the Electric Ship Research and Development Consortium (ESRDC), which was established by the Office of Naval Research (ONR) in 2002. This consortium plays a pivotal role in promoting a multidisciplinary approach to managing the system complexity inherent in an electric naval force and focuses on developing the necessary tools for complex system design and engineering to mitigate risks and reduce costs associated with early-stage decisions [3].

One such tool that seeks to propel the Navy through this evolutionary transition is the

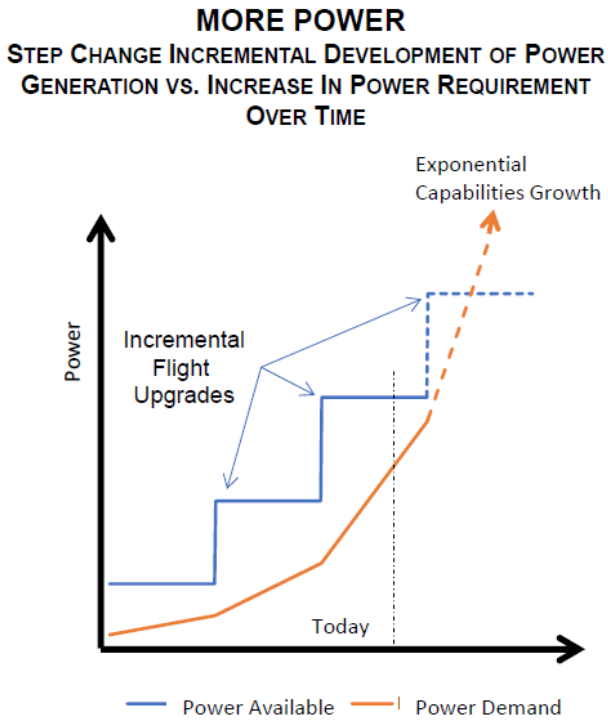

Figure 1.1: Current power systems cannot support future power demand [2]

Naval Power and Energy Systems (NPES) Technology Development Roadmap (TDR), which was developed in 2019. It outlines a strategic guide for evolving the U.S. Navy's power and energy systems and is designed to address the challenges posed by revolutionary weapon and sensor systems, as outlined in the 2018 National Defense Strategy [4]. One concept to achieve the goals outlined within the NPES TDR is the Power Electronics Power Distribution System (PEPDS).

1.2 PEPDS

PEPDS is a novel concept for power, energy, and control distribution which represents a groundbreaking development in power and energy management for various shipboard loads and ultimately seeks to deliver on the Navy's goal of all-electric ships outlined in the NPES TDR. This system leverages technology developed by the ONR, including high-power-density and high-efficiency power electronics, Silicon-Carbide (SiC) power semiconductors, and advanced tools for modeling and simulation design and analysis. Unlike the current Integrated Power and Energy System (IPES) that operates on either AC or DC power distribution, PEPDS is versatile, capable of handling both AC and DC power simultaneously from various sources. This system can efficiently control and coordinate a wide range of dynamic and stochastic loads, such as motors, radar, lasers, and any other shipboard equipment requiring power. The system's integrated control and health monitoring capability ensures that any load, regardless of whether it is AC or DC, dynamic or stochastic, receives the appropriate power and functionality [3]. The inability of legacy systems to handle both dynamic and

stochastic loads is depicted in Figure 1.2.

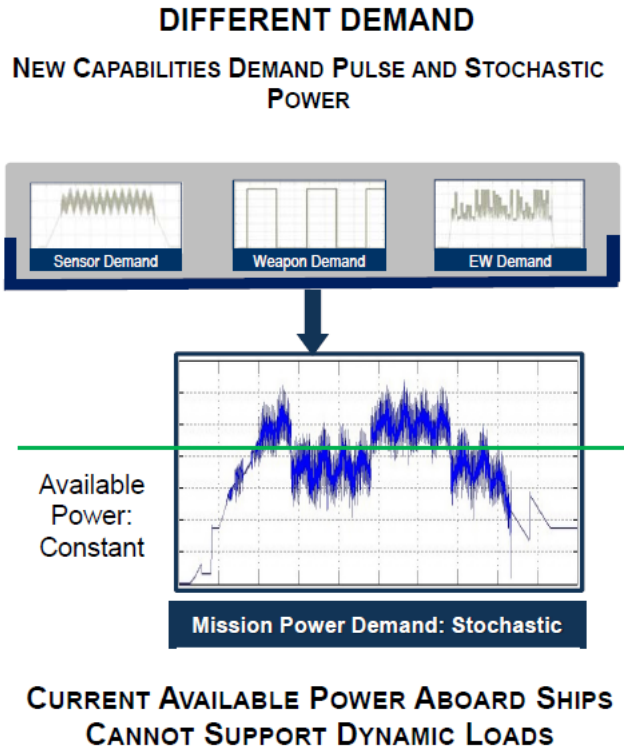

Figure 1.2: Legacy systems are unable to support both stochastic and dynamic loads [2]

The objective of the PEPDS program is to bring about revolutionary changes in system design and operation. A five-year program was proposed for the development of PEPDS and focuses on five primary areas of study: Navy Integrated Power and Energy Corridor (NiPEC), integrated Power Electronics Building Block (iPEBB), Model is the Specification, control, and system simulation [3]. This thesis focuses on the NiPEC and iPEBB.

1.2.1 NiPEC

The NiPEC introduces a significant leap in coordinating power distribution for naval applications, fundamentally changing how a ship's electrical distribution system is built. As a single modular entity, NiPEC integrates all essential components for power distribution including main bus cables, conversion, protection, isolation, control systems, and energy storage [3]. This integration marks a significant advancement over the legacy IPES, as NiPEC is capable of handling a full range of power conversions (AC-AC, AC-DC, DC-AC, DC-DC). Furthermore, NiPEC is considered reserved space in the ship's design process, ensuring adequate allocation for electrical power generation and distribution. The corridor can be customized to specific watertight subdivisions or compartments within the ship, allowing for co-located sources and loads to determine the necessary space [5]. Previous studies have assumed a four-corridor layout throughout the ship, and this assumption was carried forward for this thesis. The generalized layout of NiPEC in a notional destoryer-type ship is depicted in Figure 1.3.

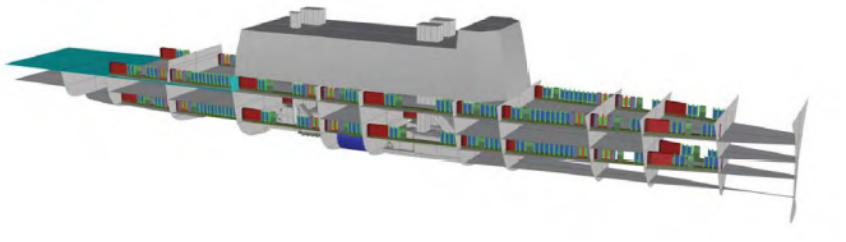

Figure 1.3: Profile View of NiPEC in Notional Ship [5]

This design philosophy enhances reliability through redundant power sources and incorporates energy storage within the power corridor through the use of energy banks or magazines, providing a power reservoir for pulse-load weapons and enabling various efficient electrical plant operations, such as in-port battery operations. The corridor's design prioritizes resilience, with co-located supporting components and geographically separated redundant elements, ensuring that a single component failure doesn't compromise the entire system. Additionally, it enhances sailor safety by confining all electrical connections and equipment within a defined, enclosed space and includes integral internal services like cooling to meet its operational requirements [3].

1.2.2 iPEBB

Within the NiPEC system, the iPEBB functions as a modular universal converter that is power-dense, self-contained, and portable by a single sailor. These identical units can handle various types of power conversion, including AC-AC, AC-DC, DC-AC, DC-DC, resulting in the ship containing hundreds of these uniform modules instead of numerous bespoke units [1]. Multiple integrated Power Electronics Building Blocks (iPEBBs) can be combined to meet any power conversion need on the ship, with their specific functions configured through software upon insertion into the system. The iPEBBs utilize SiC semiconductor technology, which offers more efficient and dynamic performance compared to traditional Silicon-based devices, with benefits like higher breakdown voltage, faster switching speeds, lower switching losses, and higher operating temperatures [6].

Within the NiPEC system, the iPEBB is designed to be the least replaceable unit, simplifying maintenance and repair operations by replacing the whole unit instead of individual components, thus minimizing system downtime. Its modular design and software control enable easy replacement, and the commonality among units reduces the need for diverse parts procurement and storage, also simplifying user training. The current design iteration of the iPEBB is approximately 550 mm in length, 300 mm in width, and 100 mm in height, with a weight of around 35 pounds. This size and weight make it manageable for a sailor to carry and install onboard a ship. The internal layout and dimensions of the iPEBB, hereafter referred to simply as PEBB, are depicted in Figure 1.4 and underpin this technology's utility and flexibility in naval power systems [3] [7].

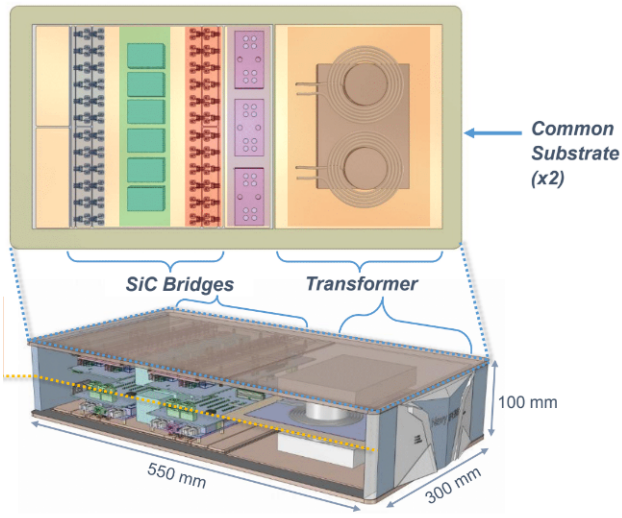

Figure 1.4: Navy iPEBB [8]

1.3 Problem Statement

While the PEBB promises high power efficiency in its conversion and storage functions, it still faces significant thermal management challenges due to heat dissipation from electrical losses, primarily from the heat generated by Metal-Oxide-Semiconductor Field-Effect Transistors (MOSFETs) [9]. These challenges are further compounded by the specific constraints of the NiPEC design. Key constraints include the compactness of the power corridor, which limits space for cooling equipment; the need for modularity and the ability for sailors to easily insert and remove PEBB units; and the requirement to avoid placing cooling water connections near electrical components, which effectively rules out direct liquid cooling options.

Each PEBB unit is assumed to dissipate about 10 kW of heat which must be dissipated. Additionally, thermal solutions for the PEBB must be capable of cooling multiple units simultaneously, i.e. a PEBB stack. An example of these PEBB stacks is illustrated by the columns of dark blue boxes in Figure 1.5. The design must also consider the portability requirement, favoring a small, lightweight, and a high-power density solution. Cooling mediums must be chosen carefully to avoid proximity to electrical components, as the high voltage levels of the units will require electrical isolation in both the cooling and electrical paths. The thermal management design must also facilitate easy swapping of units without requiring extensive sailor intervention for connections, beyond simple removal and insertion.

1.4 Previous Research

With the impossibility of direct liquid cooling, additional PEBB cooling strategies have been explored to include air cooling and external liquid cooling with a dry interface. While air cooling proved to be a viable option, it would require upwards of 1.3 m^2 of surface area as well as a localized cooling system for the chilled air inlet, which is infeasible for the current

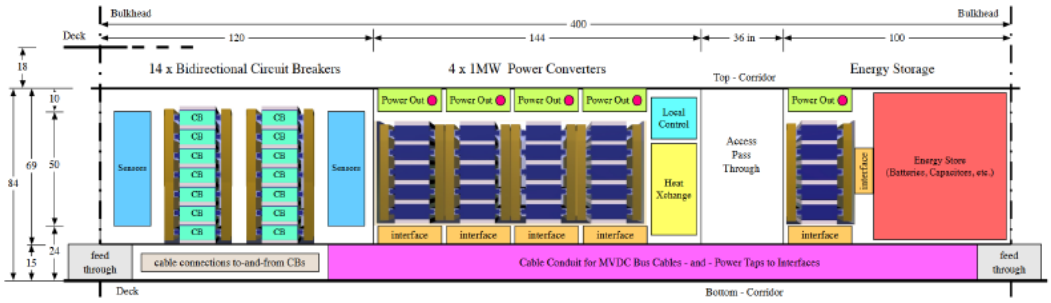

Figure 1.5: Profile View of an Example NiPEC System [1]

NiPEC design [9]. The more promising method is to cool the PEBB via an external liquid with a dry interface, in which a cold fluid is passed through inlaid copper piping within cold plates that are in contact on the top and bottom of the PEBB itself, cooling the units via conduction. This method has been demonstrated to adequately remove up to 10 kW of heat from the PEBB if a Thermal Interface Material (TIM) is present between the PEBB and cold plate, effectively lowering the contact resistance between the PEBB and the cold plate and enhancing conduction [10]. To address electrical safety concerns, deionized (DI) water or dielectric liquids, which lack electrical conductivity, will be used as cooling mediums.

Previous theses used shell-and-tube heat exchangers (STHE) for NiPEC's thermal management problem, with one design utilizing multiple STHEs to cool individual compartments on the ship and the other utilizing six STHEs to cool the entire NiPEC system (shipwide). While both of these methods were successful in providing adequate cooling to the NiPEC system, a more modular approach was desired to enable the modular construction of the NiPEC cooling system alongside the concurrent assembly of the NiPEC electrical system. Alternate methods were recommended to be researched as a result, with one of the more promising cooling methods utilizing PHE.

1.5 Thesis Outline

The primary objective of this thesis was to design and simulate a NiPEC indirect liquid cooling system, specifically tailored for efficient cooling a stack of six PEBBs. The system aims to handle a heat load of 144 kW and investigates the practicality and efficiency of using a compact PHE for this application. This cooling system is designed to integrate seamlessly with ongoing research into the PEBB and its supporting systems. The intricate design and evaluation of this compact heat exchanger are intended to comply with the modular nature of both the NiPEC cooling and electrical frameworks, facilitating simultaneous construction. Additionally, it is developed to meet the non-intrusive interface requirements and address the unique challenges posed by naval shipboard environments. Moreover, the design adheres to the standards and specifications set by the U.S. Navy, relevant shipping classification societies, and current engineering industry norms.

Drawing upon fundamental thermodynamic principles, Chapter 2 conducts an initial

assessment of employing a compact PHE for consideration within the NiPEC framework. This evaluation entails a sequence of theoretical calculations, which were subsequently fine-tuned to attain the desired objectives. The research extends upon the groundwork laid by Reyes [7] and Chaterjee [11] in their preliminary design, aiming to suggest improved architectures for cooling systems. These proposed designs are tailored to meet rigorous military standards, all the while guaranteeing resilient thermal management capabilities.

Chapter 3 endeavors to build upon the theoretical analysis outlined in Chapter 2 by elaborating on the design methodology of an innovative compact PHE. This involves utilizing SolidWorks, a Computer Aided Design (CAD) software, to facilitate the design process. The PHE will be tailored specifically to meet the cooling demands of a configuration comprising six PEBBs, collectively generating 144 kW of heat. Furthermore, this phase of the project is imperative to guarantee that the design of the new PHE aligns with the spatial limitations within the PEBB cabinet, ensuring seamless integration and optimal functionality.

Chapter 4 applies the PHE model developed in Chapter 3 to conduct multiple flow simulations, aiming to further understand the fluid dynamics at play within the PHE. A response surface model is created that illustrates how various explanatory variables, such as inlet velocity, influence response variables like the overall heat transfer coefficient of the PHE.

Chapter 5 serves as the conclusion of the thesis, outlining recommended future work and summarizing the core findings. This final chapter provides a foundation for further exploration and research based on this study's results.

Chapter 2

Thermal Analysis

In order to establish a foundational evaluation of the design features for the PHE cooling system, theoretical calculations were executed and refined to attain the targeted outcomes. These design features were determined using the specifications of the PEBBs, the spatial limitations inherent in the NiPEC, and the guidelines provided by the technical authority. Before delving into heat exchanger theory, an overview of PHE components and operation are required to establish a foundational knowledge of the cooling system.

2.1 PHE Operation

PHEs are widely utilized in marine environments, such as onboard ships, where spatial efficiency and adaptability are paramount. These exchangers operate on the same heat transfer principles as shell-and-tube units but differ significantly in structure. PHEs provide a considerably larger surface area for heat exchange compared to STHEs, resulting in more rapid and effective heat transfer. They can achieve minimal temperature differences between the cooling and cooled fluids, as low as 1°C, allowing for more compact exchanger sizes for the same heat transfer capacity [12].

The construction of PHEs involves an assembly of closely spaced, corrugated plates, each sealed with a gasket to keep the cooling and cooled fluid streams separate. This design enables counter-current flow, enhancing heat transfer efficiency while preventing fluid mixing. The plates' corrugations promote turbulent flow, which improves the exchangers overall heat transfer coefficient, though it also increases the required pumping power. Heat transfer occurs as follows: from the hot fluid to the plate by convection, through the plate by conduction, and finally to the cold fluid by convection [13].

During manufacturing, herringbone corrugations and flow channels are either stamped or cut into the plates, aiding in fluid distribution and boosting heat transfer. The plates, which can be made from a variety of materials, are arranged in the plate pack such that herringbone corrugations alternate direction with each plate. This creates spaces with varying flow thickness, generating high-velocity, turbulent flow that enhances heat transfer rates and reduces fouling by scrubbing the plates with turbulent fluids. Additionally, the flow distribution channels in the port areas ensure thorough flow across the entire plate surface to maximize heat transfer [13].

One drawback of PHEs is their higher susceptibility to fouling compared to other heat exchanger types. The flat plates, narrow gaps, and corrugations can accumulate particulates, diminishing heat transfer efficiency and necessitating more frequent maintenance. However, maintenance costs are generally lower compared to other exchangers of similar capacities, thanks to ease of disassembly and its simpler design. In PHEs, the cooling water enters through the bottom left inlet, with some fluid diverted between the plates, then returning to the outlet at the front face, while the fluid being cooled follows a similar, but opposite, path within the plates. An example PHE is shown in Figure 2.1.

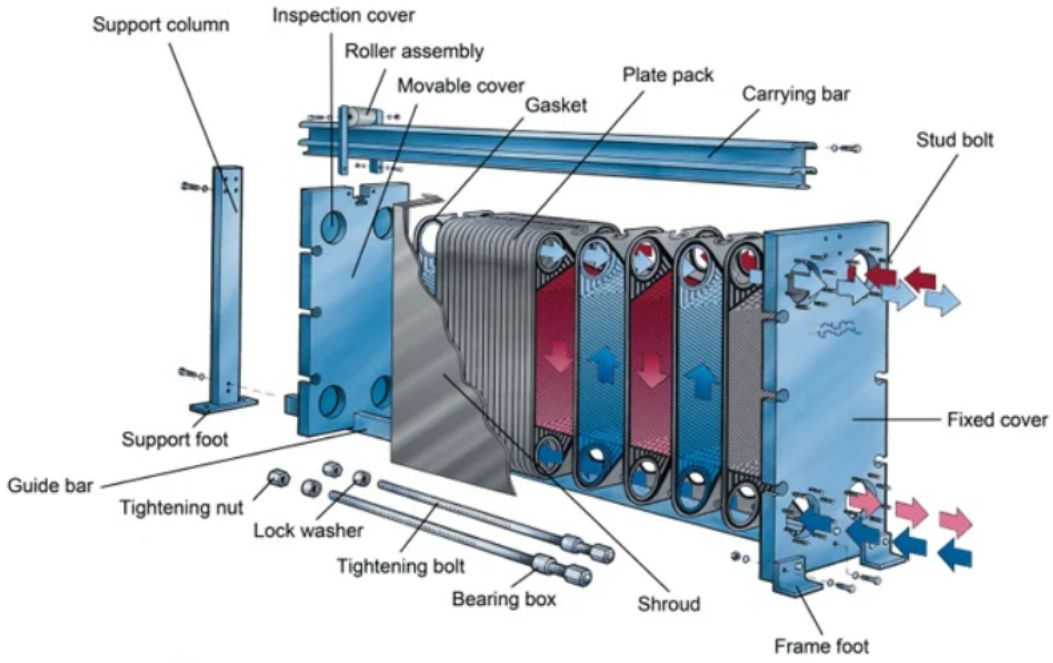

Figure 2.1: PHE Operation with Hot and Cold Flow Paths [14]

2.2 Heat Exchanger Theory and Design

The examination presented in this section adheres to conventional heat transfer methods as outlined in textbooks such as Kays and London [15]. Fourier's Law is the fundamental equation which governs heat exchanger design and is given in Equation 2.1. This equation was used in order to characterize the appropriate design criteria for the PHE, specifically calculation of the overall heat transfer coefficient (U) and the heat transfer surface area (A). These calculations are crucial for evaluating both the efficiency and the dimensions of the PHE.

$$\dot{Q} = UA\Delta T \tag{2.1}$$

where $\dot{Q}$ is the rate of heat transfer (W), U is the overall heat transfer coefficient ($\frac{W}{m^2K}$), A is the heat transfer surface area (m^2) on which U is based, and ΔT is the Logarithmic Mean Temperature Difference (LMTD) in (K). Subsequent sections detail the methodologies and formulas employed to calculate the overall heat transfer coefficient (U) and the total heat transfer surface area (A), establishing a robust groundwork for designing the PHE.

Following previous work and assumptions from [7], [10], and [11], each PEBB was assumed to generate approximately 10 kW of heat. Additionally, it is assumed that one PHE unit will provide cooling for six PEBB units, resulting in 60 kW of heat generated. Applying a safety factor of 20%, one stack of PEBBs will generate 72 kW of heat. This analysis also assumes that the PHE will be able to cool an adjacent PEBB stack for purposes of redundancy should a PHE fail, thereby resulting in a total cooling capacity for the PHE equal to 144 kW.

In order to utilize Equation 2.1 effectively, many variables had to be determined such as inlet temperatures, velocities, plate corrugation angle and aspect ratio (width-to-lenth ratio) to name a few. Determination of these variables is expounded upon in the following sections.

2.2.1 Fluid Properties

Drawing from the analysis of cold plate cooling for the NiPEC corridor system as proposed by Padilla et al. [10], the cooling water (i.e. cold leg) to the PHE will be ship's chilled water at a temperature of 7°C. For hot leg temperature, according to DOD-STD-1399 the temperature of the cooling water supplied to the inlet connections of the electronic equipment (i.e. the cold plate) on surface ships shall not exceed 40°C [16]. This is further bolstered by research from Underwood et al. [17] which shows that the required effectiveness of the cold plate is greatly increased if inlet temperature to the cold plate (i.e. PHE hot leg exit temperature) is $\leq$30°C. This is shown in Figure 2.2a. Thus, a 10°C ΔT was assumed across the heat exchanger for an inlet hot leg temperature of 40°C.

For the velocities, the assumptions from the most recent research by [7] and [11] were carried forward for the ship's chilled water, which assumed a flow rate of 2.5 $\frac{m}{s}$. For the PHE hot leg (i.e. cold plate inlet cooling water), Yang et. al [9] determined that a maximum allowable junction temperature to prevent thermal runaway within the PEBB is $\leq$200°C. Padilla et al. [10] included a safety factor of 50°C so that the maximum allowed internal PEBB temperature is 150°C and further showed that a cold plate cooling water velocity of 2.5 $\frac{m}{s}$ is adequate in order to maintain the internal PEBB components near this value of 150°C. This is shown in Figure 2.2b. Furthermore, by ensuring that the velocities of both the chilled water and the DI water are identical, equal rates of wear and tear on either side of the plate will be achieved. This symmetry will help to maintain the structural integrity and performance efficiency of the plates over time and mitigate the potential for one side to deteriorate faster than the other, which could compromise the heat exchanger's effectiveness and longevity. Achieving matched velocities is a strategic approach to prolonging the operational lifespan of the equipment and ensuring consistent, balanced thermal exchange processes. Additionally, the inlet pipe diameters for both chilled water and DI water was set to $\frac{1}{2}$ in, or 12.7 mm in accordance with the most previous research conducted by [11].

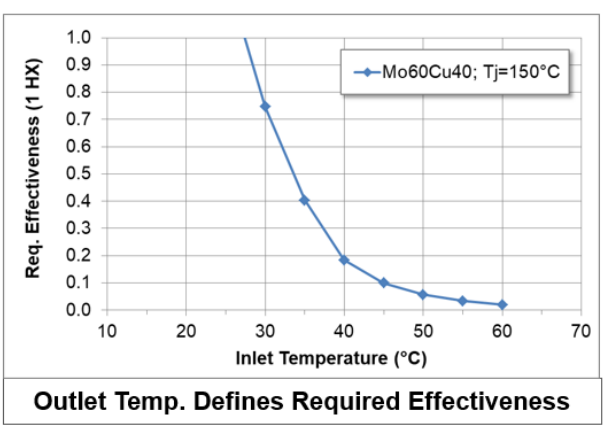

(a)

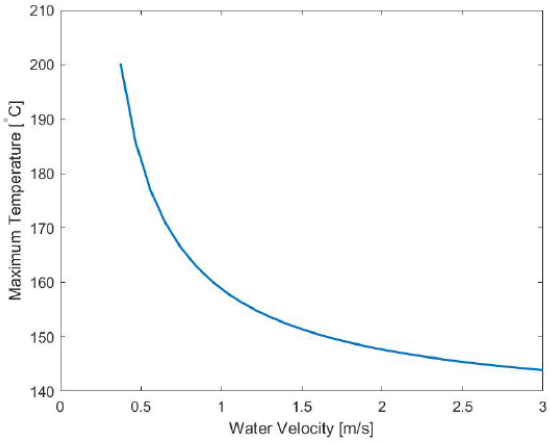

(b)

Figure 2.2: (a) Cold plate effectiveness vs. cold plate inlet temperature (i.e. PHE hot leg outlet) [17] (b) Internal PEBB temperature vs. flow rate of cold plate cooling water [10]

2.2.2 Plate Geometry and Properties

The angle of inclination (or corrugation angle) relative to the primary flow direction is a critical design factor influencing fluid friction and heat transfer. A higher corrugation angle leads to higher pressure drops, and lower corrugation angles lead to lower pressure drops as highlighted by Martin [18]. A 90° angle signifies a normal flow, meaning the flow is perpendicular to the corrugations, while a 0° angle indicates flow parallel to the corrugations. However, these extremes are seldom used in practice. The ability of a system to contain pressure is contingent on the contact points of the ridges, and the density of these contact points is maximized at a 45° angle, making it a more preferable and practical choice in design considerations [19]. Thus, a corrugation angle of 45° was chosen for this application.

The aspect ratio (width-to-length ratio) of the plates also constitutes a significant design factor. Depending on the heat transfer needs, the dimensions of the plates can vary, but they typically adopt a rectangular shape with a length approximately three times the width. Such a configuration is favored because it establishes a flow pattern that optimizes heat transfer performance [13]. In the envisioned setup, the PHE will be positioned at the base of a six-stack PEBB cabinet, shown in Figure 2.3. The base cabinet has dimensions of 406.4 mm in length, 603 mm in depth, and 647.3 mm in height [20]. To accommodate interfacing equipment, cooling cables, and the PHE frame, the plates within the PHE were designed to be 450 mm in height. In line with the previously mentioned aspect ratio, the width of the plates is consequently set at 150 mm. Additionally, the plates are designed to be thin, which serves to reduce resistance to heat transfer and also helps in maintaining a low overall weight of the unit [13]. [21] provides a range of plate thicknesses for various applications, which led to the decision to have a thickness of 2 mm for both the plate and gasket (thus the plate separation is also 2 mm). As stated in Section 1.5, the PHE cooling system is being designed to function seamlessly alongside current research on the PEBBs and associated support systems, and previous research from [7], [10], [11] utilized $\frac{1}{2}$ in (12.7 mm) for inlet flow conditions. Thus, this condition was carried forward for the PHE application.

In most naval applications, titanium is the preferred material for PHEs. Although stainless steel offers a more economical alternative, titanium plates are commonly used in Navy applications due to their superior resistance to corrosion and erosion, as well as their contribution to a substantial decrease in overall weight. Consequently, titanium was selected as the optimal metal for this application. As for the gaskets, they are made from an elastomeric material that is specifically engineered to maintain its sealing capabilities under the operating temperature and pressure conditions. High-quality rubber was chosen as the material for these gaskets, ensuring effective and durable sealing performance. Table 2.1 outlines the applicable PHE parameters and their values.

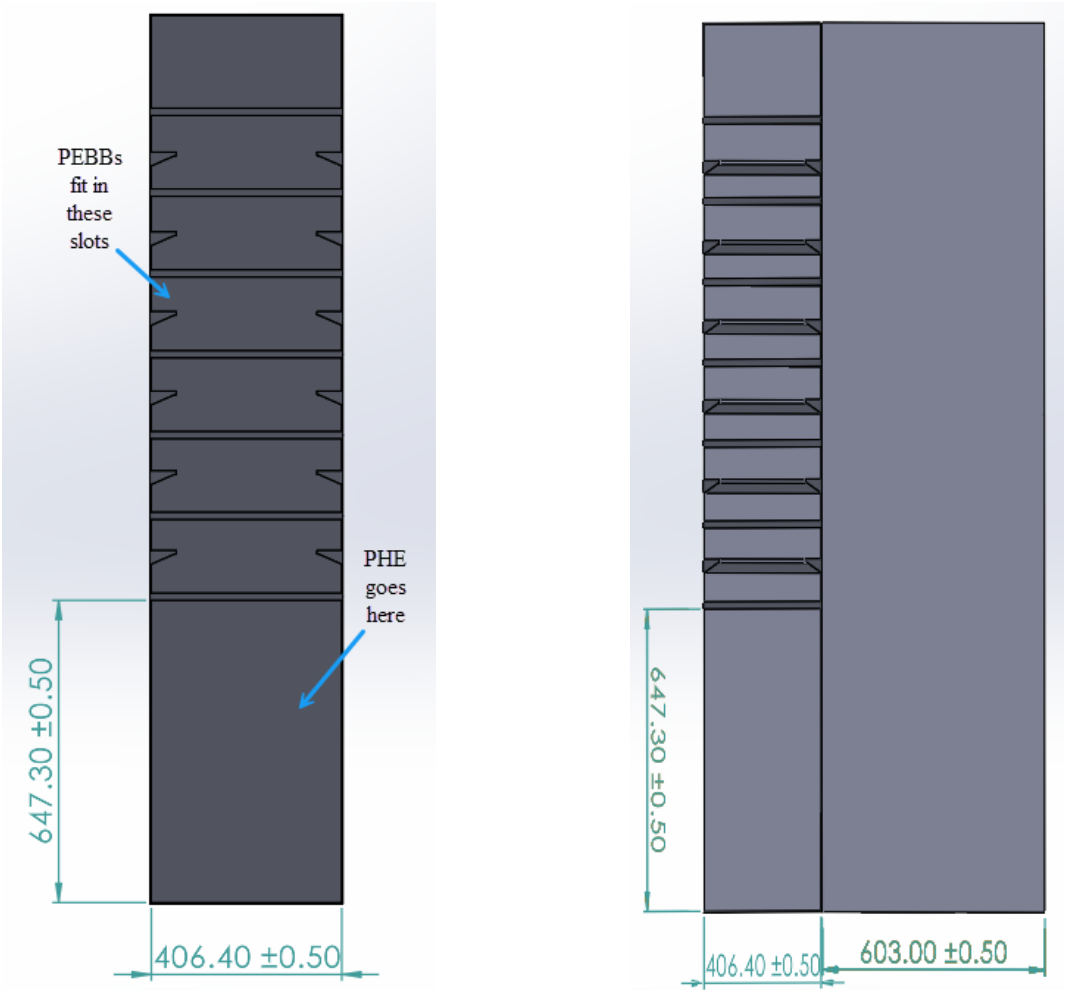

Figure 2.3: PEBB Cabinet showing space where the PHE will be positioned [20]

2.2.3 Heat Exchanger Variables Determination

Unlike STHE's, the plates utilized in PHE applications vary greatly in design and therefore can exhibit vastly different thermal characteristics. The extensive variety of plate designs, each with distinct corrugation angles (ϕ), aspect ratios and plate geometries make it challenging to establish universal, accurate correlations [21], [22]. Consequently, industry primarily

Parameter	Symbol	Value	Units
Corrugation Angle	ϕ	45	degrees (°)
Plate Length	L	450	mm
Plate Width	W	150	mm
Plate Thickness	t	2	mm
Plate Inlet/Outlet Port Diameters	d	12.7	mm
Thermal Conductivity of Titanium	k	17.0	$\frac{W}{mK}$
Plate Spacing	b	2	mm

Table 2.1: Plate Geometry and Properties

relies on specific experimental data for performance assessments, with most of this data being proprietary [19]. However, some representative performance results have been made publicly available in scholarly articles. A noteworthy set of equations, grounded in a robust mechanistic model of fluid flow, is presented by Martin [18]. This approach utilizes the generalized Lévêque solution, which pertains to the evolving thermal boundary layer alongside a developed (parabolic) velocity profile on a flat plate. In this method, the Nusselt Number, Nu, is formulated in relation to the Fanning friction factor and is shown in Equation 2.11. The Nusselt number is used to determine the convective heat transfer coefficients for both the chilled water and DI water (h_{CW} and h_{DI}, respectively) flowing over the plates, which can then be used to determine the overall heat transfer coefficient (U). In order to determine the Nusselt number, the Reynolds number and Prandtl number must first be determined.

The Reynolds number, Re, is the ratio of the inertial forces to viscous forces of a fluid and will determine whether the flow between the plates is either turbulent or laminar. For PHEs, the Reynolds number is defined in terms of the hydraulic diameter, D_h. The hydraulic diameter in a PHE is a conceptual diameter that is used to calculate the flow characteristics in non-circular tubes or channels. It is an important parameter in heat transfer and fluid dynamics as it facilitates the use of formulas originally devised for circular pipes in the context of non-circular systems. It does so by offering an equivalent diameter for these sophisticated geometries, thereby enabling a more streamlined application of these equations [21]. The Reynolds number is expressed in terms of the hydraulic diamter, D_h, using Equation 2.2 below.

$$Re = \frac{GD_h}{\mu} \tag{2.2}$$

where G is the fluid mass velocity based on the minimum free area ($\frac{kg}{m^2 s}$), D_h is the hydraulic diameter (m) and μ is the dynamic viscosity of the fluid ($\frac{Ns}{m^2}$). Shah [21] defines G as

$$G = \frac{\dot{m}}{2aW_g} \tag{2.3}$$

where $\dot{m}$ is the mass flow rate of the fluid ($\frac{kg}{s}$), a is the amplitude of the corrugation angle (m) and W_g is the width of plate between the gaskets (m).

The hydraulic diameter, D_h, as defined by Martin [18] is given by Equation 2.4 below.

$$D_h = \frac{4a}{\Phi} \tag{2.4}$$

with the area enhancement factor Φ defined as

$$\Phi = \frac{1}{6}(1 + \sqrt{1 + X^2} + 4\sqrt{1 + X^2/2}) \tag{2.5}$$

and

$$X = \frac{2\pi a}{\Lambda} \tag{2.6}$$

where X is the wave number (non-dimensional) and Λ is the wavelength of the corrugation angle across the plate (m).

To calculate the amplitude (a), width of the plate between the gaskets (W_g) and wavelength (Λ) associated with the aforementioned 45° chevron angle, a plate and gasket were modeled in the CAD software SolidWorks, employing parameters such as plate height and width as outlined in Table 2.1. The relevant values for applying Equations 2.2 through 2.6 are provided in Table 2.2, as shown below.

Parameter	**Symbol**	**Value**	**Units**
Chilled Water Mass Flow Rate	$\dot{m}_{cw}$	3.80	$\frac{kg}{s}$
DI Water Mass Flow Rate	$\dot{m}_{DI}$	3.77	$\frac{kg}{s}$
Plate Width Between Gasket	W_g	0.110	m
Amplitude of 45° Chevron Angle	a	0.045	m
Wavelength of 45° Chevron Angle	Λ	0.106	m
Chilled Water Fluid Mass Velocity	G_{cw}	381.95	$\frac{kg}{m^2 s}$
DI Water Fluid Mass Velocity	G_{DI}	379.04	$\frac{kg}{m^2 s}$
Wave Number	X	2.68	N/A
Area Enhancement Factor	Φ	1.99	N/A
Hydraulic Diameter	D_h	0.091	m
Chilled Water Reynolds Number	Re_{cw}	24252	N/A
DI Water Reynolds Number	Re_{DI}	52632	N/A

Table 2.2: Parameters for a 450 mm x 150 mm plate with a 45° chevron angle

The Prandtl number, Pr, is defined as the ratio of momentum diffusivity to thermal diffusivity. It is a function of the fluid only and not of the geometry of the application itself and is an indication of whether conduction or convection is dominant.

$$Pr = \frac{c_p \mu}{k} \tag{2.7}$$

where c_p is the isobaric specific heat of water ($\frac{kJ}{kgK}$) and k is the thermal conductivity of water ($\frac{W}{mK}$).

Having defined the Re and Pr, we can now determine Nu utilizing the approach given by Martin [18], shown as Equation 2.8 below.

$$\frac{1}{\sqrt{f}} = \frac{cos(\phi)}{\sqrt{0.045tan(\phi) + 0.09sin(\phi) + \frac{f_0}{cos(\phi)}}} + \frac{1 - cos(\phi)}{\sqrt{3.8f_1}} \tag{2.8}$$

where

$$f_0 = \begin{cases} \frac{16}{Re} & \text{for } Re < 2000 \\ \frac{1}{(1.56lnRe - 3.0)^2} & \text{for } Re \geq 2000 \end{cases} \tag{2.9}$$

and

$$f_1 = \begin{cases} \frac{149.25}{Re} + 0.9625 & \text{for } Re < 2000 \\ \frac{9.75}{Re^{0.289}} & \text{for } Re \geq 2000 \end{cases} \tag{2.10}$$

where ϕ is the corrugation angle in degrees, f is the Fanning friction factor and both f_0 and f_1 are ancillary friction factors.

The correlation for the Fanning friction factor as defined by Equations 2.8 through 2.10 applies to corrugation angles between 0-80°, with its accuracy spanning from -50% to +100% [18]. It is worth noting that the precision of this correlation could be significantly enhanced by the availability of detailed geometrical information.

Once the overall friction factor is found using the above equations, the Nusselt Number Nu can be found using Equation 2.11.

$$Nu = 0.205Pr^{\frac{1}{3}}(\frac{\mu}{\mu_w})^{\frac{1}{6}}(fResin(2\phi))^{0.374} \tag{2.11}$$

where μ_w is the dynamic viscosity of the fluid at the wall. This correlation applies to corrugation angles ranging from 10-80°, with an accuracy of ±30% [21].

Using this correlation, the definition of the Nusselt number is used to determine the convective heat transfer coefficients for chilled water and DI water (h_{CW} and h_{DI}, respectively). The Nusselt number is defined as the ratio of convection to conduction across a boundary and is shown in Equation 2.12 below.

$$Nu = \frac{hD_h}{k} \tag{2.12}$$

where h is the convective heat transfer coefficient ($\frac{W}{m^2K}$), D_h is the hydraulic diameter (m) used in Equation 2.2 and k is the thermal conductivity of the fluid ($\frac{W}{mK}$). The values of h_{CW} and h_{DI} are listed in Tables 2.3 and 2.4, respectively.

After calculating the convective heat transfer coefficients for both chilled water and DI water, Equation 2.1 can be reformulated in accordance with the definition of the overall heat transfer coefficient (U) as presented in Equation 2.13 [23].

$$U = \frac{\dot{Q}}{A\Delta T} = \frac{1}{\frac{1}{h_{CW}} + \frac{L}{k} + \frac{1}{h_{DI}}} \tag{2.13}$$

where L is the plate width (m) and k is the plate material in ($\frac{W}{mK}$). Referencing the discussion in Section 2.2.2, titanium was chosen as the preferred material due to its array of advantages

Parameter	Symbol	Value	Units
Inlet Temperature	T_{cin}	7.0	°C
Density	ρ	999.86	$\frac{kg}{m^3}$
Velocity	v	2.5	$\frac{m}{s}$
Reynolds Number	Re	24252	N/A
Dynamic Viscosity	μ	$1.43x10^{-3}$	$\frac{Ns}{m^2}$
Specific Heat Capacity	c_p	4200	$\frac{J}{kgK}$
Thermal Conductivity	k	0.574	$\frac{W}{mK}$
Friction Factor, f_0	f_0	$6.15x10^{-3}$	N/A
Friction Factor, f_1	f_1	0.527	N/A
Fanning Friction Factor	f	0.194	N/A
Prandtl Number	Pr	10.46	N/A
Nusselt Number	Nu	462.33	N/A
Chilled Water Heat Transfer Coefficient	h_{CW}	2922.72	$\frac{W}{m^2K}$

Table 2.3: Chilled Water Parameters

Parameter	Symbol	Value	Units
Inlet Temperature	T_{hin}	40.0	°C
Density	ρ	992.25	$\frac{kg}{m^3}$
Velocity	v	2.5	$\frac{m}{s}$
Reynolds Number	Re	52632	N/A
Dynamic Viscosity	μ	$6.59x10^{-4}$	$\frac{Ns}{m^2}$
Specific Heat Capacity	c_p	4180	$\frac{J}{kgK}$
Thermal Conductivity	k	0.6286	$\frac{W}{mK}$
Friction Factor, f_0	f_0	$5.13x10^{-3}$	N/A
Friction Factor, f_1	f_1	0.421	N/A
Fanning Friction Factor	f	0.188	N/A
Prandtl Number	Pr	4.35	N/A
Nusselt Number	Nu	608.48	N/A
Deionized Water Heat Transfer Coefficient	h_{DI}	4212.52	$\frac{W}{m^2K}$

Table 2.4: Deionized Water Parameters

for PHE applications. The value of U was calculated to be 1487.8 $\frac{W}{m^2K}$ and is listed in Table 2.5.

The final calculation made before establishing the value of A was the LMTD, ΔT, given by Equation 2.14.

$$\Delta T = \frac{(T_{hin} - T_{cout}) - (T_{hout} - T_{cin})}{ln(\frac{T_{hin} - T_{cout}}{T_{hout} - T_{cin}})} \tag{2.14}$$

In this context, T_{hin} represents the inlet temperature of the DI water, T_{hout} denotes the outlet

temperature of the DI water (and thus the inlet to the cold plate), T_{cin} refers to the inlet temperature of the chilled water, and T_{cout} is the outlet temperature of the chilled water. T_{cin} and T_{hin} are listed in Tables 2.3 and 2.4, respectively, and T_{hout} was set to a value of 30°C . The selection of these values was discussed in Section 2.2.1.

To ascertain the value of T_{cout}, Equation 2.1 was reformulated to incorporate mass flow rate and can be recast as Equation 2.15 below.

$$\dot{Q} = \dot{m}_{cw} c_p \Delta T_{cw} = \dot{m}_{cw} c_p (T_{cin} - T_{cout}) \tag{2.15}$$

where $\dot{Q}$ represents the rate of heat transfer (W), $\dot{m}$ denotes the mass flow rate of chilled water (kg/s), and c_p signifies the specific heat capacity of water $(\frac{J}{kgK})$. These values are specified in Tables 2.2 through 2.5. By rearranging this equation, T_{cout} was determined to be 18.43°C.

Subsequently, the LMTD was computed utilizing Equation 2.14, resulting in a ΔT of 22.28°C. By inputting all the presently determined values into Equation 2.1 and reorganizing the equation to isolate A, the total necessary heat transfer surface area for the plate heat exchanger was determined to be 0.328 m^2. An overview of the key parameters and geometries of the PHE is presented in Table 2.5.

Parameter	**Symbol**	**Value**	**Units**
Heat Transfer Rate	$\dot{Q}$	144	kW
LMTD	ΔT	22.28	K
Plate Length	L	0.450	m
Plate Width	W	0.150	m
Plate Thickness	t	0.002	m
Inlet/Outlet Port Diameter	d	0.013	m
Hydraulic Diameter	H_d	0.091	m
Thermal Conductivity of Plate	k	21.6	$\frac{W}{mK}$
Chilled Water Heat Transfer Coefficient	h_{CW}	2922.72	$\frac{W}{m^2K}$
Deionized Water Heat Transfer Coefficient	h_{DI}	4212.52	$\frac{W}{m^2K}$
Overall Heat Transfer Coefficient	U	1487.8	$\frac{W}{m^2K}$
Plate Surface Area	A	0.328	m^2

Table 2.5: PHE Characteristics

The calculated values for U and A suggest potential for high efficiency and an appropriately sized PHE for NiPEC consideration. However, the cumulative error arising from the application of Equation 2.8 in conjunction with Equation 2.11 has the potential to introduce substantial inaccuracies.

To illustrate the impact of these inaccuracies, calculations for the maximum potential overestimation and underestimation were conducted and are shown in Equations 2.16 and 2.17.

$$Maximum\ Overestimation = [Value] * 2 * 1.3 = [Value] * 2.6 \tag{2.16}$$

where "2" is a result of the maximum positive error in Equation 2.8 (+100%) and "1.3" is a result of the maximum positive error in Equation 2.11 (+30%). This yields a compounded error of +160%, or 2.6 times the actual value.

$$Maximum\ Underestimation = [Value] * 0.5 * 0.7 = [Value] * 0.35 \tag{2.17}$$

where "0.5" is a result of the maximum negative error in Equation 2.8 (-50%) and "0.7" is a result of the maximum negative error in Equation 2.11 (-30%). This yields a compounded error of -65%, or 0.35 times the actual value.

While the outcomes derived from the aforementioned correlations appear promising and offer a solid foundation for the initial design of the PHE, they carry the risk of considerable error stemming from the notable inaccuracies inherent in these correlations. As a result, it is advised against solely using these equations for detailed modeling of a PHE in the context of NiPEC designs. To more accurately evaluate the performance of a PHE within the NiPEC system, a tailored design of a PHE was initiated, followed by conducting flow analyses under various conditions, such as different inlet temperatures and flow rates. This approach is expected to deliver more reliable outcomes and enhance understanding of the operational dynamics of the PHE. The methodologies and findings from this investigation form the core of Chapter 3.

Chapter 3

PHE Design

As referenced in Chapter 2, the diversity in design of plates used within PHE applications introduces significant variability in their thermal performance characteristics. This stems from a wide range of corrugation angles, aspect ratios, and plate geometries, complicating the development of universally applicable and accurate thermal performance correlations [21], [22]. The model introduced by Martin [18] exhibited considerable inaccuracies ranging from -65% to +160%, which presents significant risk should these equations be used as the sole basis for effectively integrating the PHE into the NiPEC model.

Leading PHE manufacturers provide a wide selection of plates featuring different sizes, heat transfer surface areas, and corrugation patterns, allowing for customization to specific thermal demands and sizing constraints [22]. Their reliance on empirical data and flow simulations for PHE performance evaluation underscores the need for a tailored approach with regard to the NiPEC cooling system model. Therefore, the development and simulation of a novel PHE were deemed essential for precisely evaluating the cooling requirements for a configuration of six PEBBs, which collectively produce 144 kW of heat. Additionally, this process was necessary to ensure the new PHE's design would comply with the spatial constraints of the PEBB cabinet. This section details the design methodology of a new PHE, employing the CAD software SolidWorks for the design process.

3.1 Plate Design

The plates constitute the core component of the plate heat exchanger, serving to direct the flow of both hot and cold fluids and facilitate the heat transfer process between them. Several of the assumptions introduced in Chapter 2 were adopted as foundational elements in the design process of the PHE using SolidWorks, providing a solid baseline for plate development. To reiterate, the PEBB base cabinet's dimensions are specified as 406.4 mm in length, 603 mm in depth, and 647.3 mm in height, as depicted in Figure 2.3 [20]. The PHE plates were crafted with a height of 450 mm, providing approximately 8 inches of clearance above the heat exchanger for connecting equipment, cooling cables, and the PHE framework. Consistent with earlier discussions, the plates generally exhibit a rectangular shape, with their length about three times their width, a design choice that enhances the flow pattern to optimize heat transfer efficiency as noted in [13]. Accordingly, the width of

the PHE was determined to be 150 mm, a dimension that not only augments heat transfer efficacy but also ensures sufficient room for the integration of connecting apparatus within the base of the PEBB cabinet. To maximize heat transfer and maintain a low overall weight for the unit, the plates were designed with a thin profile. This approach aligns with the assumption outlined in Chapter 2, which specified a plate thickness of 2 mm, and this specification was carried forward into the design.

A crucial aspect affecting the performance of the PHE is the chevron (or corrugation) angle in relation to the primary direction of fluid flow. The corrugation patterns featured on the plates of PHEs serve to induce turbulence within the fluid flows, and this turbulence enhances convective heat transfer which enables PHEs to reach higher efficiency levels compared to traditional STHEs [24]. As Martin [18] indicates, higher corrugation angles result in increased pressure drops, while lower angles are associated with decreased pressure drops. The effectiveness of the PHE in containing pressure is significantly influenced by the contact points along the ridges of the corrugation angles, with the density of contact points reaching its peak at a 45° angle [19]. This makes the 45° chevron angle a favorable and practical selection for design consideration and seeks to minimize pressure drop throughout the exchanger.

Plate manufacturers for PHEs can either cut into or emboss the plates to create the requisite chevron angles. Embossing involves stamping the chevron angle corrugations and flow channels directly into the plates, which offers the added benefit of increasing the structural integrity of the plate [13]. However, Equation 2.1 illustrates that the heat transfer rate ($\dot{Q}$) is directly proportional to the heat transfer surface area (A). Consequently, it was decided to form the chevron angles by cutting into the plates, a method that effectively increases the heat transfer surface area available on each plate and leads to a significant improvement in the overall rate of heat transfer.

The depth of the corrugation angle must also be considered, with shallower corrugations typically accumulating less residue due to the turbulence they generate in fluid flow. Moreover, fabricating plates with deeper corrugations poses considerable challenges, as noted in [25]. Given that the plate thickness is set at 2 mm, a corrugation depth of 0.75 mm was selected for each side of the plate. This choice maximizes heat transfer across the plate by maintaining a minimal separation of only 0.5 mm between the hot and cold fluids while still maintaining the plate's structural integrity.

The surface area for fluid flow on one side of the plate was calculated to be 36,464 mm^2, and introducing a single chevron cut adds 289.16 mm^2 to the plate's surface flow area. By implementing forty chevron cuts on one side of a plate, the surface area designated for heat transfer is enhanced by 31.7% compared to a surface that lacks corrugations produced through cutting techniques. As noted in [22], it is established that modifications to the heat transfer surface area can be made in discrete increments, each equivalent to the surface area of a single plate. Based on the aforementioned area calculations, the cumulative surface area available for heat transfer within the PHE, denoted as A in Equation 2.1, can be accurately calculated using the formula presented in Equation 3.1.

$$A = 0.0845 * \textit{Number of plates in PHE} \tag{3.1}$$

where A is in m^2.

As noted in the Naval Ship's Technical Manual (NSTM) 505 [26], the selection of a piping system's diameter is influenced by the pressure drop, which is dictated by the system's available pressure head and its flow requirements. The velocity to be used in these determinations is often at the discretion of the designer. In alignment with ongoing research on PEBBs and their support systems, and drawing from prior studies by [7], [10], [11], a $\frac{1}{2}$ in (12.7 mm) diameter was chosen for both inlet and outlet flow conditions in the PHE cooling system design. This decision, however, imposes restrictions on acceptable velocities at the inlet and outlet, which take into account the characteristics of the materials used and the objective to mitigate the erosion of system components. This limits the maximum allowable velocity to 1.28 $\frac{m}{s}$ (4.2 $\frac{ft}{s}$). This is illustrated in Figure 3.1 below.

Table 505-5-1. FLUID VELOCITY LIMITS

Pipe Size (NPS)	Velocity (fps)	Flow (gpm)
1/2	4.2	5.2
3/4	4.8	9.9
1	5.4	18.6
1-1/4	6.2	34.9
1-1/2	6.6	49.8
2	7.4	88.4
2-1/2	8.2	147
3	9.1	244
3-1/2	9.8	348
4	10.3	462
5	11.5	794
6 and larger	12.0	1187

Figure 3.1: Maximum Allowable Fluid Velocities for Various Pipe Diameters [26]

It is well established in literature that with increased velocity comes increased turbulence, which thereby increases the overall heat transfer rate within the PHE [13], [21], [24]. Given the velocity restrictions at the PHE's inlet and outlet, there was a clear intention to augment fluid turbulence within the inter-plate spaces. To achieve immediate turbulence enhancement as the fluid initially contacts the plate surface, approximately 100 dome-shaped perturbations were introduced on each plate's face at the fluid inlet. These are shown at the bottom of Figure 3.2a and at the top of Figure 3.2b, within the diamond-shaped inlet plenum region. These dome-shaped modifications also share the 0.75 mm depth characteristic of the chevron angle cuts, ensuring consistency in design. The inclusion of these perturbations represents a straightforward modification for manufacturers, increasing the plates' appeal due to the anticipated improvements in heat transfer efficiency.

As detailed in Chapter 2, titanium was selected as the preferred material for the plates, a decision that was incorporated into the SolidWorks modeling. Although stainless steel offers a more economical alternative, titanium plates are commonly used in U.S. Navy applications due to their superior resistance to corrosion and erosion, as well as their contribution to a substantial decrease in overall weight. To illustrate the weight difference, a forty-plate PHE was modeled in SolidWorks using both stainless steel (AISI 316) and titanium. The

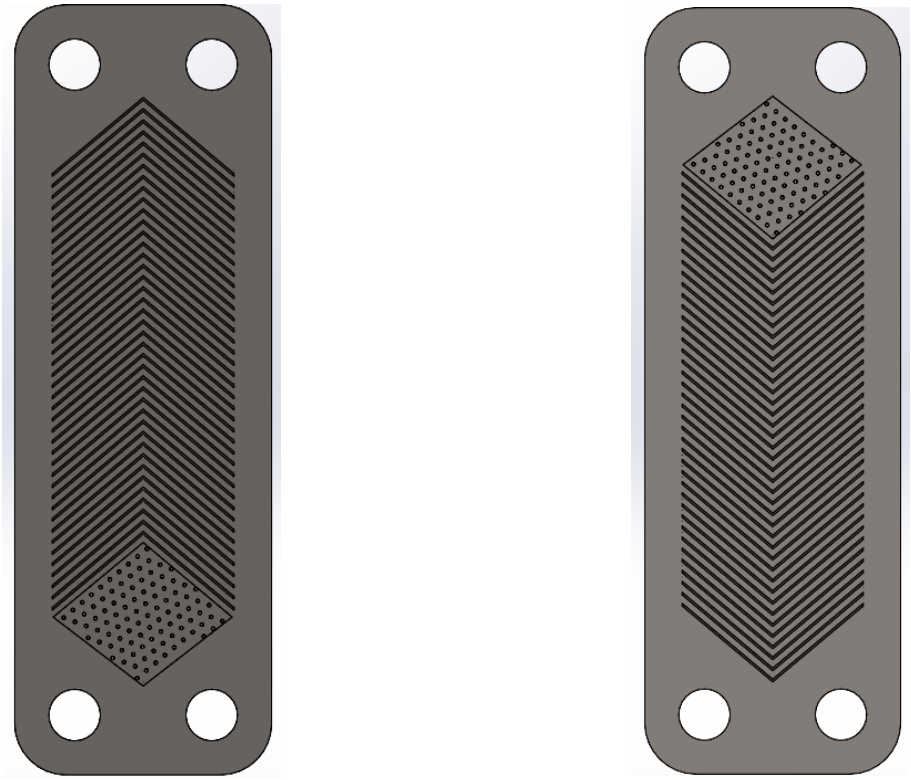

(a) Front of Plate (Chill Water Flow)

(b) Back of Plate (DI Water Flow)

Figure 3.2: Plates are the single most important determination of PHE efficacy

completed model revealed that the stainless steel PHE weighed 125.48 pounds, whereas the titanium model weighed 87.51 pounds. As a result, opting for titanium as the material for the plates results in a significant weight reduction of 30.3%.

The final plate design for the PHE is modeled in Figure 3.2a and Figure 3.2b. It is important to note that the PHE design intentionally incorporates a solid final plate at the end of the PHE, devoid of any holes. Fluid encountering this plate is simply redirected towards the corresponding fluid's outlet. This design consideration aims to prevent the stainless-steel frame at the PHE's terminus from undergoing unnecessary thermal stresses during operation [13]. Additionally, the first plate in the plate heat exchanger stack has all four port holes fully enclosed by the gasket, which prevents the fixed frame from experiencing similar thermal stresses. Both of these considerations are visually depicted by the simplified flow pattern shown in Figure 3.3.

3.2 Gasket Design

The design of gaskets within the PHE is as critical as the design of the plates themselves. Surrounding the edge of each plate, the gaskets are positioned to encapsulate either the DI or the chill water inlet and outlet ports. These gaskets, when compressed against the subsequent plate, serve to contain the fluid within the plate pack, preventing leaks [13].

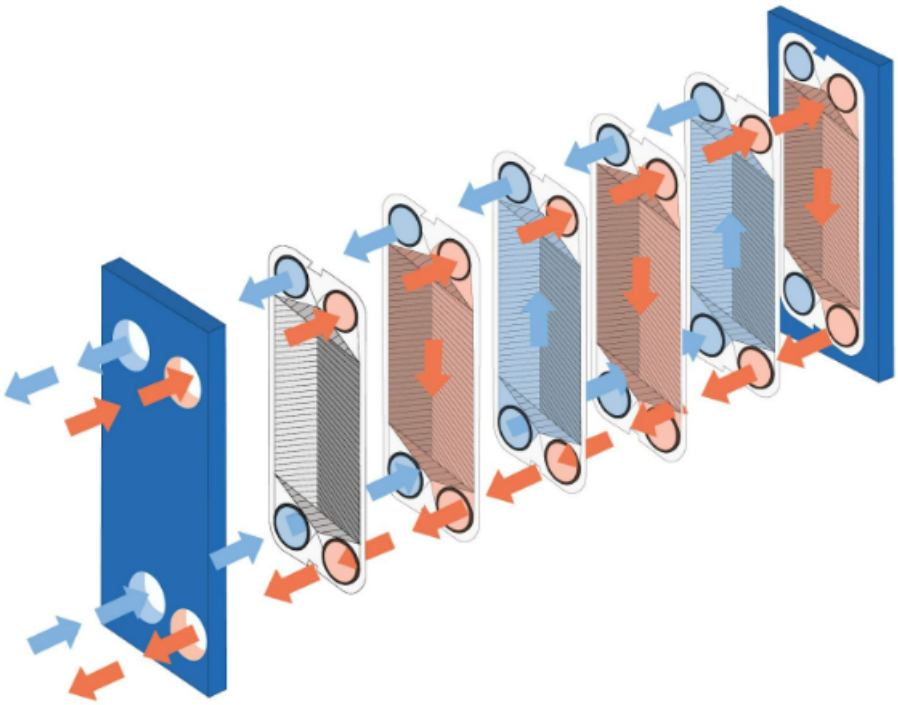

Figure 3.3: Fluid flow paths inside a PHE [27]

Additionally, they dictate the flow path of the DI or chill water between the plates they adjoin, based on the configuration of circled ports and those left open. On each header, the ports were configured such that they are alternately enclosed by a gasket or left open, directing the fluid to flow through every alternate space. For example, for gaskets where the DI water ports are open, the corresponding chill water ports are sealed, ensuring that only DI water passes through the space between plates and chill water does not. This configuration creates the requisite alternating pattern of DI water and chill water, essential for effective heat transfer. The gaskets were affixed into pressed grooves around the perimeter of the plates using the *Mating* feature in SolidWorks (not shown in Figures 3.2a nor 3.2b), ensuring accurate placement and stability under operational pressures.

Consistent with previous discussions in Section 2.2.2, the gaskets were crafted in SolidWorks using an elastomeric material, specifically high-quality natural rubber. Selected for its exceptional durability and sealing capabilities, high-quality natural rubber excels in enduring the demands of continuous use, particularly the stresses from repeated thermal cycling. This resilience minimizes the necessity for regular maintenance and replacements. Moreover, its application involves exposure to ship's chilled water and DI water, environments that do not necessitate the enhanced chemical resistance characteristics of materials like nitrile or butyl rubber. Furthermore, this choice is economically advantageous, offering a cost-effective solution without compromising on the essential sealing and performance qualities when compared to alternative gasket materials.

Figure 3.4 enumerates common gasket materials alongside their application spectrum [21]. The gaskets were engineered to maintain their sealing efficacy under the specific temperatures and pressures encountered during PHE operation. Notably, gasket durability often sets the

boundaries for the PHE's maximum operational conditions. Utilizing natural rubber as the gasket material of choice sets the maximum operating temperature of the PHE application at 70°C. Consistent with the discussion in Section 2.2.1, a 10°C ΔT was assumed across the cold plate (i.e. T_{hin}=40°C), which incorporates a safety margin of 30°C.

Gasket Material	Generic Name	Maximum Operating Temperature (°C)	Applications	Comments
Natural rubber	*cis*-1,4-polyisoprene	70	Oxygenated solvents, acids, alcohols	
SBR (styrene butadiene)		80	General-purpose aqueous, alkalies, acids, and oxygenated solvents	Has poor fat resistance
Neoprene	*trans*-1,4-polychloroprene	70	Alcohols, alkalies, acids, aliphatic hydrocarbon solvents	
Nitrile		100–140	Dairy, fruit juices, beverage, pharmaceutical and biochemical applications, oil, gasoline, animal and vegetable oils, alkalies, aliphatic organic solvents	Is resistant to fatty materials; particularly suitable for cream
Butyl (resin cured)		120–150	Alkalies, acids, animal and vegetable oils, aldehydes, ketones, phenols, and some esters	Has poor fat resistance; suitable for UHT milk duties; resists inorganic chemical solutions up to 150°C
Ethylene propylene (EDPM) rubber		140	Alkalies, oxygenated solvents	Unsuitable for fatty liquids
Silicone rubber	Polydimethyl-siloxane	140	General low-temperature use, alcohols, sodium hypochlorite	
Fluorinated rubber		175	High-temperature aqueous solutions, mineral oils	

Figure 3.4: Common Gasket Materials for PHEs [21]

Figure 3.5a demonstrates how gaskets are positioned to enable the flow of chilled water while preventing the flow of DI water. To reverse this functionality—allowing DI water to flow while blocking chilled water—the gasket needs only to be rotated 180° about its vertical axis. Except for the initial and final gaskets in the assembly, all gaskets are uniform throughout the unit. The first and last gaskets, illustrated in Figure 3.5b, distinguish themselves by encompassing the plate's perimeter with seals around all four ports, thus preventing any fluid contact with the stationary and movable frames at both ends of the PHE. This design is intentional, safeguarding the frames from thermal stresses. In alignment with the assumptions outlined in Chapter 2, the thickness of the gaskets was determined to be 2 mm. This dimension was designed to facilitate sufficient fluid flow between the plates, up to 1.25 $\frac{m}{s}$, thereby optimizing heat transfer efficiency while remaining within the constraints set by [26].

The addition of a dual-seal feature around the sections with closed ports was incorporated into the gasket design, which significantly reduces the risk of fluid leakage and inter-fluid mixing. This dual-seal acts as an extra layer of protection, particularly in the event that the internal (circular) gasket fails. To enhance the detection of potential gasket failures, the area between the seals is designed to vent externally, offering a visual cue for leakage. While these venting points are too small to be shown in Figures 3.5a and 3.5b, the overarching principle is demonstrated in Figure 3.6.

3.3 End Frames, Tie Bolts and Nozzles

The PHE features two main structural components at its ends: a fixed frame and a movable frame, both constructed from high-quality steel for durability and structural integrity. The fixed frame, typically anchored permanently to a foundation like the deck or equipment skid, will be attached to the base of the PEBB cabinet in this design, providing a stable backing

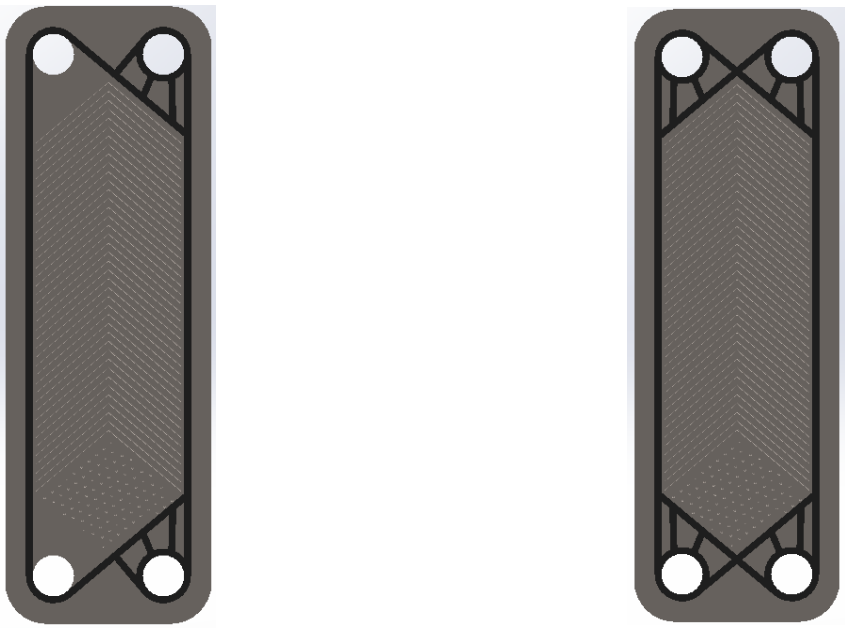

(a) Chillwater Gasket (b) Four Port Plate Gasket (shown on front plate)

Figure 3.5: Gaskets often set the limits for PHE's maximum operational conditions

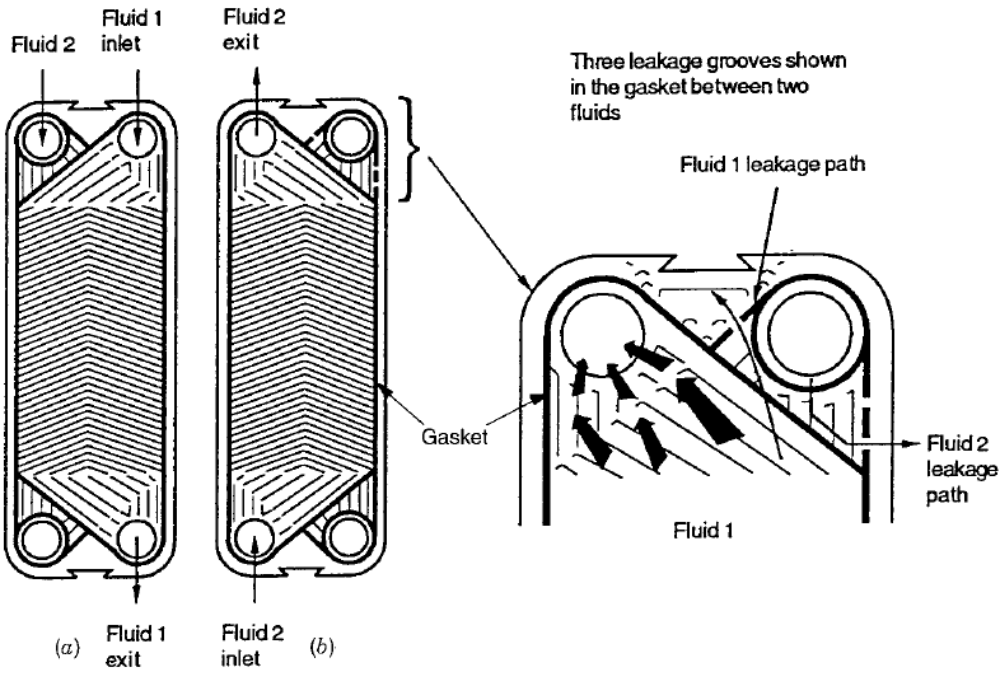

Figure 3.6: Dual-seal prevents fluid intermixing and incorporates leak detection [21].

for plate pack tightening. The fixed frame and moveable frame are depicted in Figures 3.7a and 3.7b, respectively.

The nozzles, designed as compact pipe sections, direct both chilled and DI water to their respective areas within the PHE. They are commonly equipped with flanges at their outer

ends for seamless integration with the piping system, and they protrude through the frame and are aligned with the four-port gasket on the first plate. To ensure corrosion resistance, the nozzle materials were chosen to match the fixed frame's high-quality steel construction. In the standard designs used by the Navy, all four nozzles are positioned on the fixed frame, a design choice also replicated in the SolidWorks model to eliminate the need for detaching pipes to reach the plate pack [13].

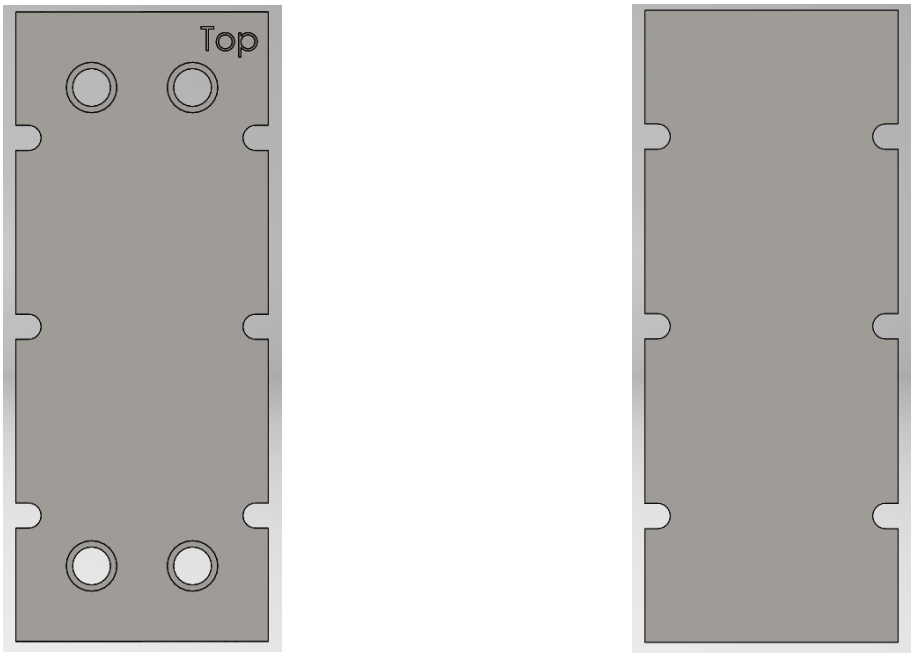

(a) Front Frame (Fixed) with Nozzles (b) End Frame (Moveable) with No Holes

Figure 3.7: The end frames are constructed from high-quality steel for durability and structural integrity

Tie bolts were incorporated to link the movable frame to the fixed frame, compressing the plate pack between them upon tightening. The gaskets were precisely engineered to create a leak-proof seal by compressing slightly to avoid warping the plates. These bolts slide into horizontal slots on the frames for straightforward disassembly, enabling hassle-free access to the plate pack for periodic maintenance requirements. A specific sequence during tightening or loosening will ensure uniform compression and prevent damage to the plates and gaskets [13].

The movable frame acts as a rear support for the plate pack, moving closer to the fixed frame as the tie bolts are tightened, thus securing the plate pack at its intended thickness. This frame glides along guide/carrying bars, positioned above the PHE, to facilitate this movement as shown in Figure 2.1.

3.4 Final Model

After the individual elements of the PHE were designed and modeled, these components were integrated to create a comprehensive model of the PHE assembly. Figure 3.8 below

depicts a PHE consisting of 30 plates. As discussed earlier, the placement of the PHE will be at the base of the PEBB cabinet, with both the fixed and moveable frames aligned axially along the cabinet's length. This alignment facilitates the attachment of the nozzle flanges (not illustrated in Figure 3.8) to the cabinet's framework securely. This configuration proves beneficial for maintenance activities, including the cleaning or replacement of plates and gaskets. By simply loosening the tie bolts and adjusting the PHE's movable frame, maintenance tasks can be performed efficiently without the necessity of dismantling the entire unit.

The PEBB cabinet's base measures 406.4 mm in length, 603 mm in depth, and 647.3 mm height [20]. The 30-plate PHE model under consideration measures 210 mm in length (spanning from the nozzle tips to the movable end plate), 200 mm in depth, and 500 mm in height. Should there be a requirement for more plates, the PEBB cabinet's base can accommodate up to 75 plates, underscoring the design's scalability and adaptability to varying thermal management needs. For example, a 40-plate PHE positioned inside the PEBB cabinet at various angles is illustrated in Figure 3.9 below.

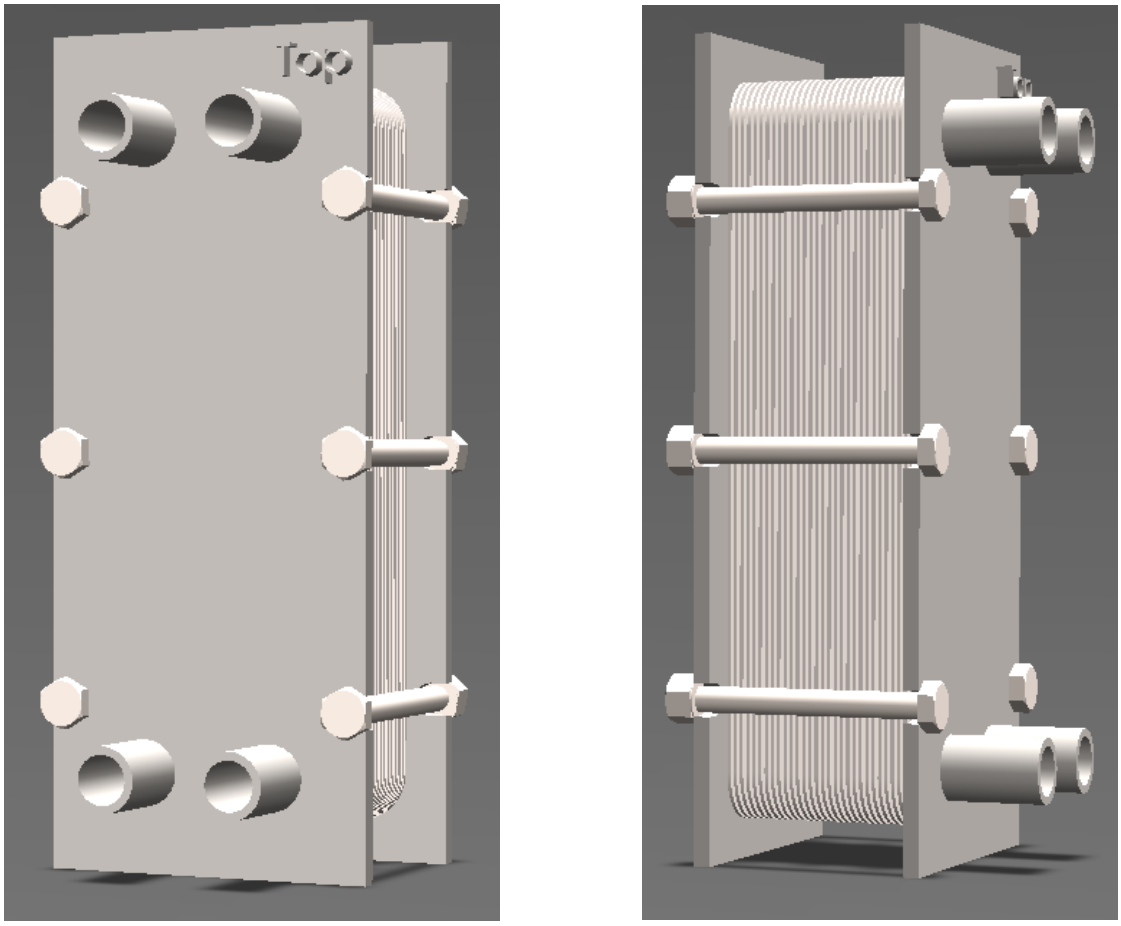

Figure 3.8: 30-plate PHE as modeled in SolidWorks

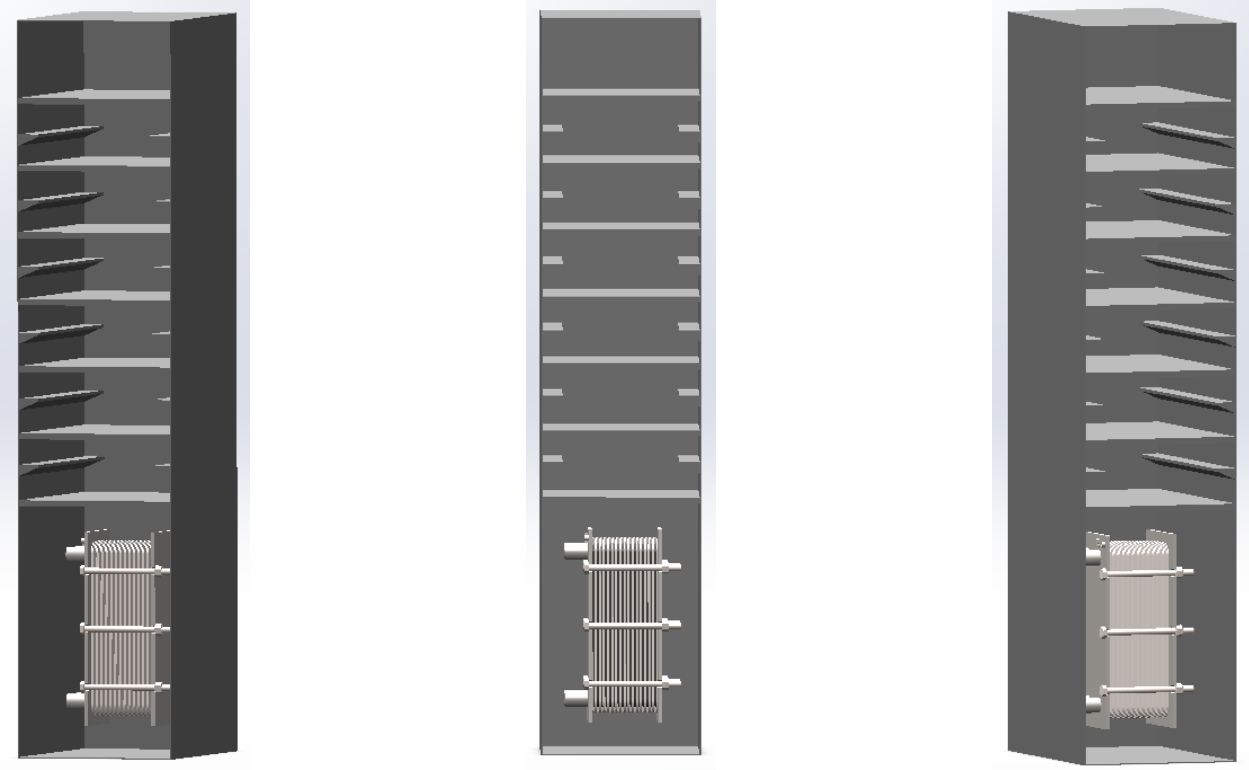

Figure 3.9: 40-plate PHE positioned inside the PEBB cabinet (shown at various angles)

3.5 System Architecture

Following the design of the comprehensive PHE model, its incorporation into the overall cooling system architecture with the PEBB cabinet represents the culmination of the process. The foundational architecture for the NiPEC cooling system, proposed by [7] and [11], served as the bedrock for integrating the PHE. Within this modular system, the primary components—namely the pump, expansion tank, resin bed, piping, fittings, and the PHE itself—are pivotal. Each component is detailed further in the subsequent sections. It is important to highlight that the discussion herein pertains exclusively to the flow path of DI water within the system. This specificity is due to the extensive utilization and well-established framework of chilled water systems, which already have a strong foundation for implementation.

A one-line diagram of the proposed system is illustrated by Figure 3.10 [28].

Pump

Within the PEBB cooling system, the pump plays a crucial role by generating the necessary force to maintain a steady flow of cooling fluid (i.e. DI water) to the electronic components throughout the system. For Navy shipboard electronic cooling water systems, centrifugal pumps are preferred due to their efficiency in moving large volumes of fluid at lower viscosities. These pumps are valued for their simpler, more compact design and their ease of maintenance compared to positive displacement pumps. Furthermore, the centrifugal pump

design allows for straightforward adjustments to the flow and pressure characteristics of the system. Consequently, any further analysis of the NiPEC cooling system will proceed with the assumption that centrifugal pumps are employed for its operational needs, which agrees with the findings by Reyes [7].

Expansion Tank

The expansion tank functions as a closed-shell water reservoir. It plays a multifaceted role in ensuring the system's efficiency and stability. Firstly, it provides a Net Positive Suction Head (NPSH) to the pump, which is essential for maintaining the pump's operational integrity and preventing cavitation—a condition where vapor bubbles form in the liquid near the pump impeller, potentially causing damage. Additionally, the expansion tank compensates for system losses by supplying make-up water in the event of gasket failure or component leaks. This capability is crucial for maintaining the fluid level within the system, ensuring that it operates within its designed parameters and preventing potential issues related to low fluid levels, such as pump overheating or failure.

Another vital function of the expansion tank is to mitigate the thermal expansion and contraction of the DI water. As the DI water heats up or cools down, it expands or contracts, respectively. The expansion tank accommodates these volume changes, thereby preventing excessive pressure buildup or vacuum conditions that could compromise system components or affect performance. By balancing these volume fluctuations, the expansion tank maintains the system's pressure equilibrium and ensures its long-term reliability and efficiency.

Ion Exchanger

An ion exchanger resin bed is utilized for regulating the chemistry of the water, specifically aiming to preserve or improve the purity of DI water. This enhancement is achieved by circulating the DI water through the resin beds, which are designed to remove compounds and debris that could induce corrosion or wear. In the process of ion exchange, all inorganic salts are eliminated from the DI water. A mixed-bed resin employs cations to transform dissolved salts in the water into acid, which the anions within the resin then capture and retain. Lowering the ion concentration in the DI water significantly diminishes the likelihood of electrical current transmission from a PEBB that possesses an external shell potential. This process is pivotal for enhancing the electrical safety and operational reliability of the system, ensuring minimal risk of electrical interference or unintended conduction, which could stem from the presence of ions in the water.

To safeguard downstream components from potential damage, mechanical filters are employed to remove particulate matter from the coolant. Such particulates can cause harm to pump bearings and valve seats through impingement or the friction that occurs between surfaces at a microscopic level. Additionally, particulates have the tendency to accumulate in the system's bends, elbows, and narrow passages, leading to flow restrictions and gradual system degradation. By addressing these concerns, the system ensures the longevity and efficiency of its operation, maintaining the high performance of the cooling system.

Pipes, Tubing and Fittings

The PEBB cooling system architecture employs pipes, tubing, and fittings crafted from copper alloy or stainless steel, adhering to the Nominal Pipe Size (NPS) and Pipe Schedule (SCH) standards for specifying their dimensions, and this study assumes the use of SCH 40 piping for all conducted piping analyses. Following the insights presented by Reyes [7], Copper-Nickel (CuNi) alloys were identified as the optimal material for the cooling circuit, owing to their exceptional flow performance and resistance to corrosion. While CuNi alloys are recommended for most components, tin bronze is advised for use in bearings and pump impellers due to its superior wear resistance. Additionally, using dissimilar metals in pipes, tubes, and fittings with water flowing through them can cause galvanic corrosion. This phenomenon occurs when metals with different electrochemical potentials are in electrical contact with an electrolyte, such as water. The more anodic metal will corrode faster than it would alone, while the more cathodic metal will be protected from corrosion. This can lead to premature failure of the system components, potentially causing leaks or other failures. To mitigate this, dielectric couplings or joints may be used, which break the electrical path between dissimilar metals. Since the NiPEC cooling architecture employs DI water, it minimizes concerns related to galvanic corrosion.

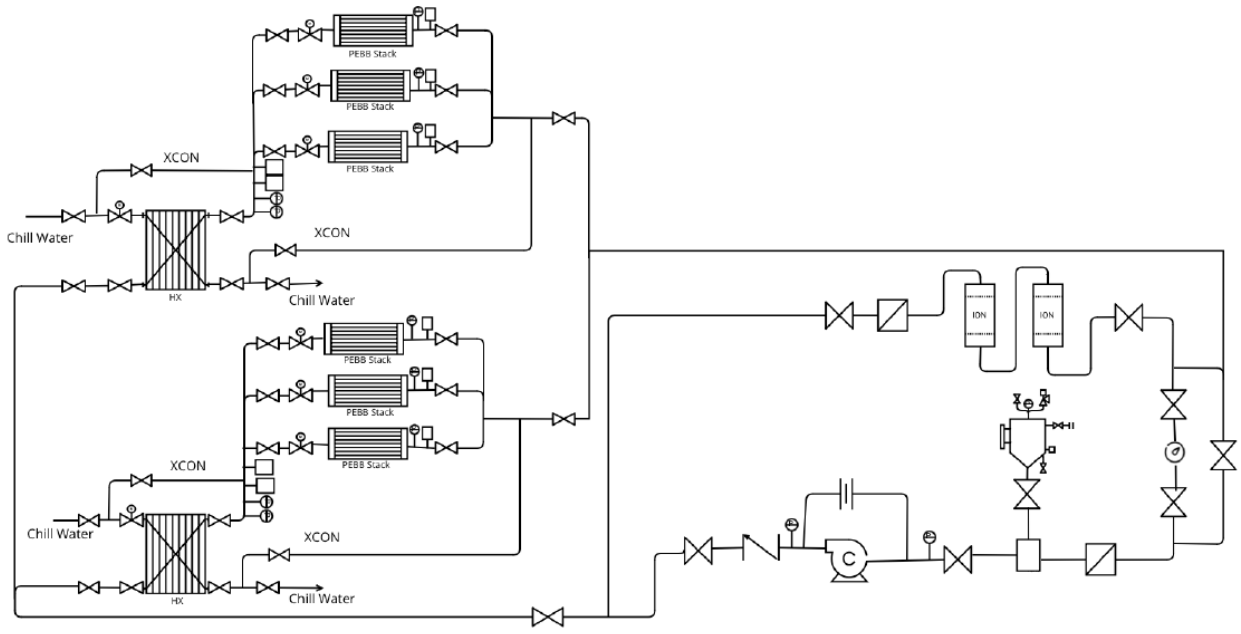

Figure 3.10: One-line diagram of the proposed NiPEC cooling system utilizing PHEs [28]

Chapter 4

Flow Simulation Analysis

As annotated in Section 1.5, the principal objective of this thesis was to theorize, design, and simulate an innovative liquid cooling system for the NiPEC. This system must be engineered for the effective cooling of a stack of six PEBB units, with a focus on dissipating a substantial thermal load of 144 kW efficiently. A pivotal aspect of achieving this goal is influenced by the findings from research conducted by Underwood et al. [17], whose studies have demonstrated a significant enhancement in the cooling performance of the cold plate when the cooling water inlet temperature — the DI water exiting the PHE — remains at or below 30°C (Figure 2.2a). Consequently, the ideal design of the PHE would not only capably manage the dissipation of 144 kW of heat but also ensure that the water supplied to the cold plate maintains a temperature of 30°C or lower.

However, given that the NiPEC and PEBB technologies are in the throes of research and development, with potential changes to their specifications anticipated, designing a PHE solely for current specifications without considering future adaptability is unwise. The design considerations, including inlet velocity, temperatures, and plate count, depend on the PEBB stack's location within the vessel and the electrical requirements of each compartment within the ship. These variables, largely at the discretion of the designer, influence the heat exchanger's efficiency, output temperatures, and overall size.

In light of these considerations, a series of flow analyses have been undertaken. The purpose of these analyses is to deepen the understanding of the thermodynamic processes involved with the designed PHE model. By doing so, once the specific electrical requirements for a compartment - and thus the necessary cooling requirements - are identified, the PHE can be tailored to align with these unique specifications. This approach underscores a commitment to flexibility and adaptability in the design process, enabling the creation of a cooling solution that is not only efficient and effective but also versatile enough to meet future needs as technologies and requirements evolve.

4.1 Boundary Conditions

When defining the boundary conditions for the PHE, selecting factors that directly influence the primary objective—namely the heat transfer rate—is paramount. This approach necessitates a review of Fourier's Equation, as detailed in Section 2.2:

$$\dot{Q} = UA\Delta T \tag{4.1}$$

This equation relates the rate of heat transfer ($\dot{Q}$) to the overall heat transfer coefficient (U), the heat transfer surface area (A), and the LMTD (ΔT). This framework enables the designer to set boundary conditions that will directly result in a greater rate of heat transfer within the PHE, as detailed further below.

The overall heat transfer coefficient, U, is notably dependent on fluid velocity. This dependency arises from the convection heat transfer coefficient, h, a critical component in U's calculation as outlined in Equation 2.13. The convection heat transfer coefficient escalates with an increase in fluid velocity, thereby boosting U. This effect is attributed to the enhanced fluid mixing at higher velocities, which diminishes the thermal boundary layer's thickness where the temperature gradient is most intense, thus enabling more effective heat transfer.

Furthermore, it has been shown from Equation 3.1 that adjustments to the designed PHE's heat transfer surface area (A) of a PHE can occur in specific increments, each corresponding to the surface area provided by a single plate. Consequently, incorporating additional plates elevates the total heat transfer surface area, which is directly proportional to the heat transfer rate ($\dot{Q}$). Accordingly, simulations were executed to explore a range of plate counts, varying from 12 to 40 plates, to assess their impact on heat transfer efficiency.

Lastly, the inlet temperatures of both the chilled water (cold leg) and DI water (hot leg) significantly affect the LMTD (ΔT), as previously illustrated in Equation 2.14. Specifically, an increase in either the DI water inlet temperature or the chilled water inlet temperature leads to a higher LMTD. Aligning with analyses by [7] and [11], the inlet temperature of the chilled water was consistently maintained at 7°C. This falls significantly beneath the mandated specifications outlined in MIL-STD-15730, which stipulates that the temperature of the cooling water for large surface vessels must remain below 95°F (35°C) [29].

Although the DI water inlet temperature is not directly adjustable by the operator, it was postulated in Section 2.2.1 that there is a temperature differential of 10°C across the cold plate, which could vary based on the power demands from the PEBBs, resulting in either a lower or higher $\Delta T_{ColdPlate}$. Consequently, simulations to investigate the effect of varying inlet temperatures for DI water were performed, covering a range from 35°C to 45°C.

The summary of the flow simulation boundary conditions are shown in Table 4.1.

Boundary Condition	**Symbol**	**Range**	**Units**
Chilled/DI Water Inlet Velocity	v_{in}	0.5 - 1.25	m/s
DI Water (Hot Leg) Inlet Temperature	T_{hin}	35 - 45	°C
Number of Plates	N_p	12 - 40	N/A

Table 4.1: Flow Simulation Boundary Conditions

4.2 Analyses

The PHE was designed and modeled using the CAD software SolidWorks, and its performance was evaluated through the Computational Fluid Dynamics (CFD) Flow Simulation add-on feature within the same software. Raw data from the various analyses is presented in Appendix B.

Various types of graphics, including cut, contour, surface, and vector, were generated to analyze the system under different boundary conditions. For the sake of brevity, only the SolidWorks graphics corresponding to a fluid inlet velocity of 1.25 $\frac{m}{s}$, a DI water (hot leg) inlet temperature of 45°C, and a configuration of 40 plates are displayed below.

4.2.1 Velocity Analysis

As discussed in Section 3.1, the maximum inlet velocities for both hot and cold streams are limited to 1.28 $\frac{m}{s}$, constrained by the inlet nozzle diameters, a limitation that was depicted in Figure 3.1. Consequently, simulations were conducted for inlet velocities ranging from 0.5 to 1.25 $\frac{m}{s}$ for both chilled and DI water, aligning with the specifications set forth by MIL-DTL-15730 [29]. These specifications and the imposed limitations are further detailed in Figure 4.1. In the simulations conducted, the velocities of both chilled water and DI water were synchronized to guarantee uniform wear and tear on both sides of the PHE plates. This approach ensures a balanced distribution of mechanical stresses and prolongs the lifespan of the PHE by maintaining even conditions across its structure.

TABLE I. Maximum cooling water velocities.

Coolant and method of supply	Velocity through inlet flange, feet per second	Velocity through tubes, feet per second
Seawater, supplied by scoop injection	11.0	9.0
Seawater, otherwise supplied	9.0	7.5
Fresh water, however supplied	11.0	9.0

Figure 4.1: Maximum Cooling Water Velocites for Surface Coolers [29]

Figures 4.2 and 4.3 illustrate the chilled and DI water velocities as they flow through the PHE with an inlet velocity of 1.25 $\frac{m}{s}$. It is noteworthy that both fluids exhibit low velocities as they navigate through the spaces between the plates of the PHE. This observation suggests that the PHE is likely to operate quietly, with minimal noise production.

As alluded to Section 4.1, the overall heat transfer coefficient (U) is influenced by fluid velocity. An increase in fluid velocity positively affects the convective heat transfer coefficient (h) by improving the mixing of the fluid adjacent to the heat transfer surface. This

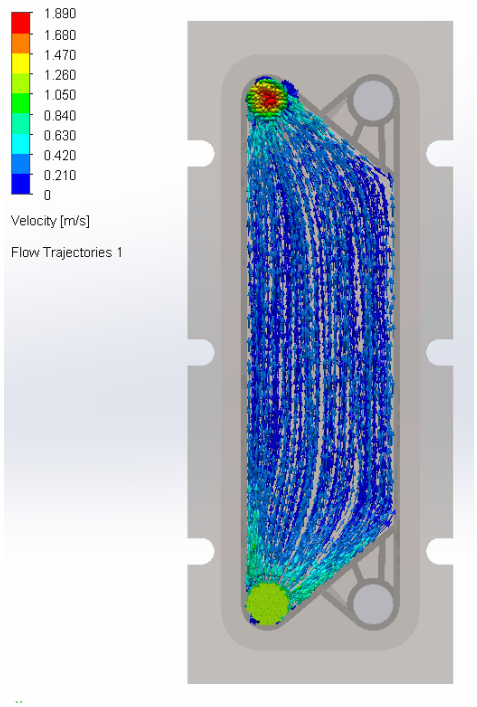

(a) Chilled Water Flow (bottom to top)

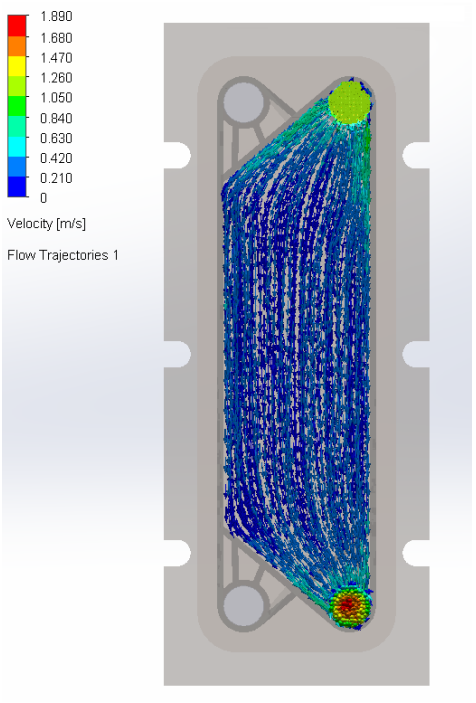

(b) DI Water Flow (top to bottom)

Figure 4.2: Front view of velocity variation in 40-plate PHE with v_{in}=1.25 m/s, T_{hin} = 45°C

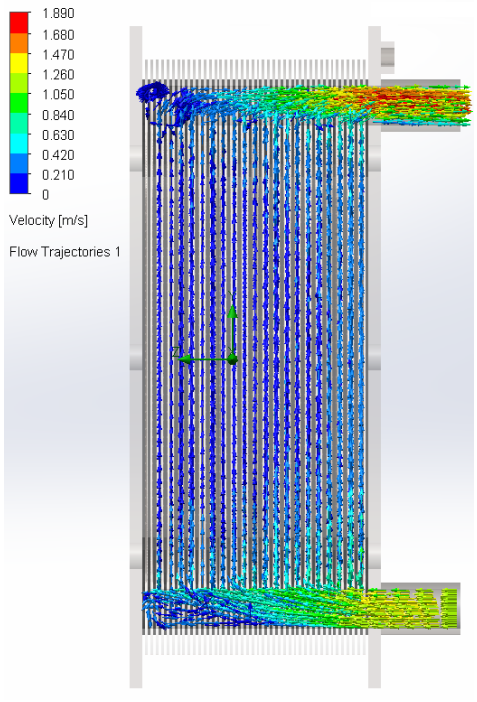

(a) Chilled Water Flow (bottom to top)

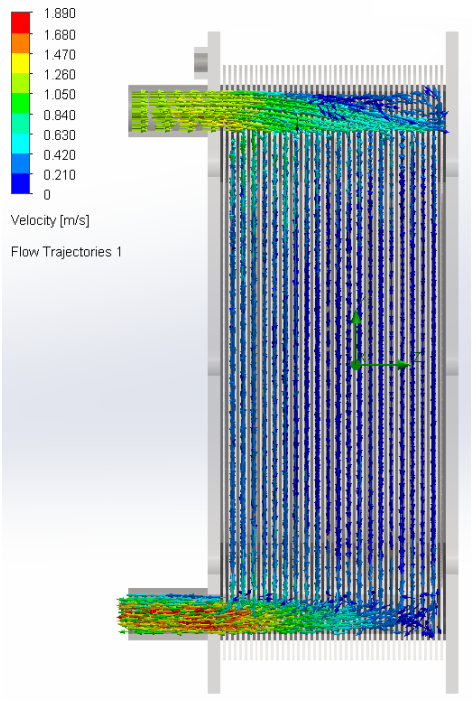

(b) DI Water Flow (top to bottom)

Figure 4.3: Side view of velocity variation in 40-plate PHE with v_{in}=1.25 m/s, T_{hin} = 45°C

improvement leads to a reduction in the thickness of the thermal boundary layer, the zone with the highest temperature differential, thereby making the heat transfer process more efficient. Therefore, increased velocities lead to a higher overall heat transfer coefficient, demonstrated in Figure 4.4.

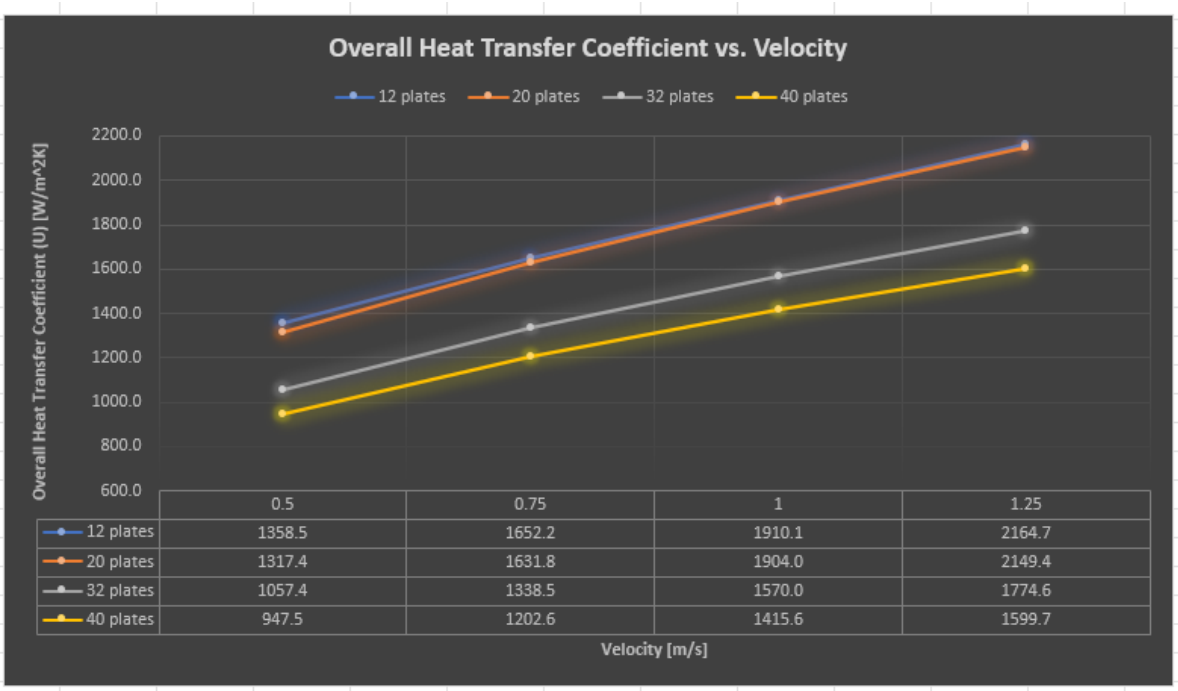

	0.5	0.75	1	1.25
12 plates	1358.5	1652.2	1910.1	2164.7
20 plates	1317.4	1631.8	1904.0	2149.4
32 plates	1057.4	1338.5	1570.0	1774.6
40 plates	947.5	1202.6	1415.6	1599.7

Figure 4.4: Overall Heat Transfer Coefficient at various v_{in} and N_p with T_{DIin}=45°C

An insight from Figure 4.4 reveals that the overall heat transfer coefficient tends to decrease as the number of plates within the PHE increases, a phenomenon that can primarily be attributed to a decrease in fluid velocity. Introducing more plates into the PHE causes the fluid to be spread across a broader surface area, leading to a decrease in velocity through the channels between plates. The flow simulation data presented in Figure 4.5 substantiates this observation, illustrating the internal velocity variations within different configurations of the PHE. Specifically, it shows that the average internal velocity in a 12-plate PHE fluctuates between 0.63 and 0.84 $\frac{m}{s}$. In contrast, the 40-plate PHE demonstrates a significantly lower average internal velocity, which is less than 0.21 $\frac{m}{s}$. Both configurations had $v_{in} = 1.25\ \frac{m}{s}$. This reduction in velocity decreases turbulence within the fluid, and consequently, reduces the convective heat transfer coefficient (h), thereby reducing the overall heat transfer coefficient U. This variance in internal velocities underscores the impact of PHE design on fluid dynamics and efficiency, revealing how additional plates can influence the flow rate and ultimately the overall heat transfer coefficient within the system.

These insights highlight the complex interplay between the design variables of a PHE and its operational effectiveness, underscoring the need for careful optimization to achieve the desired thermal performance.

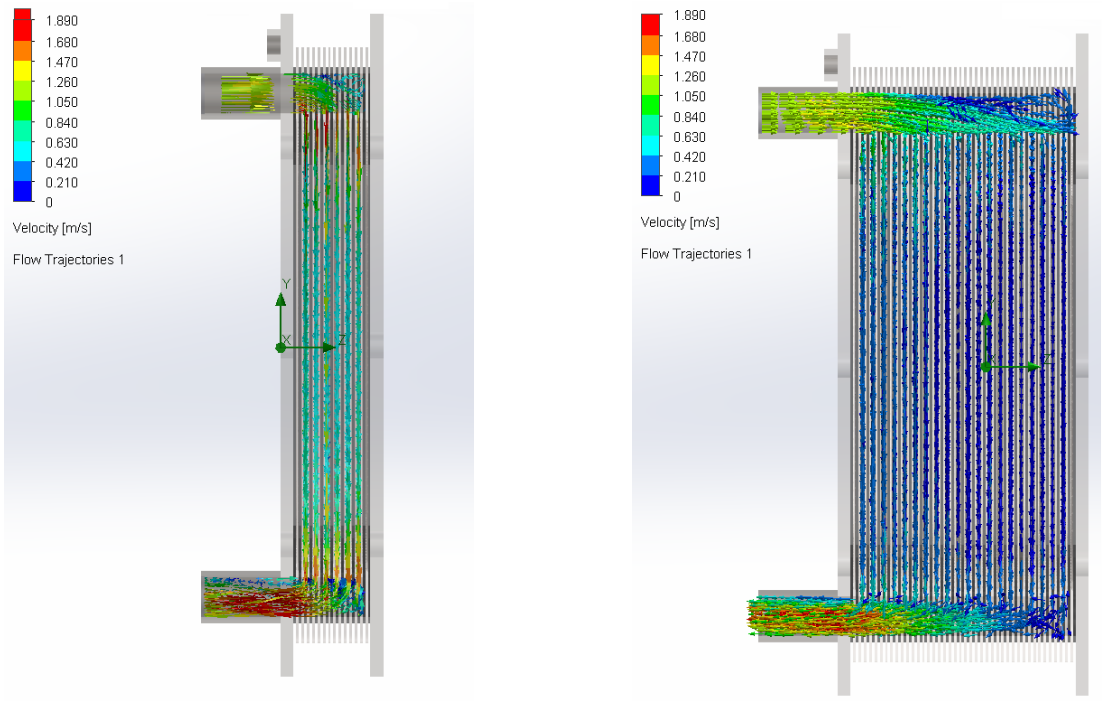

(a) DI Water Flow velocity across 12 plates (b) DI Water Flow velocity across 40 plates

Figure 4.5: Velocity variation of 12-plate PHE versus 40-plate PHE with v_{in}=1.25 m/s

4.2.2 Temperature Analysis

Figures 4.6 and 4.7 presented below depict the temperature variation of chilled and DI water as they pass through a 40-plate PHE. In these illustrations, both fluids are entering the PHE at a velocity of 1.25 $\frac{m}{s}$, with the DI water entering the heat exchanger at a temperature of 45°C. Notably, the exit temperature of the DI water falls beneath the target temperature of 30°C, which aims to maximize the effectiveness of the cold plate as referenced in Figure 2.2a.

Furthermore, Figure 4.8 demonstrates the variation in exit temperature of DI water, initially entering at 45°C, as influenced by changes in both the number of plates and the inlet flow velocities to the PHE. The graph presents findings that align with expectations: lower DI water outlet temperatures are achieved at reduced velocities, since the reduced flow rate allows the DI water more time within the system to engage in heat transfer, which also leads to a corresponding rise in chilled water outer temperatures. Although the lower DI exit temperatures enhance the efficiency of the cold plate as referenced in Figure 2.2a, a notable drawback is the corresponding decrease in the LMTD, as detailed by Equation 2.14. This reduction in LMTD, in turn, lowers the overall rate of heat transfer. Therefore, this analysis highlights the critical importance of striking an optimal balance between achieving desirable DI water outlet temperatures—for maximizing cold plate efficiency—and maintaining an adequate overall heat transfer rate to comprehensively meet the system's requirements.

Appendix C illustrates DI water outlet temperature across various PHE plate stacks and velocities for DI inlet temperatures of 35°C and 40°C.

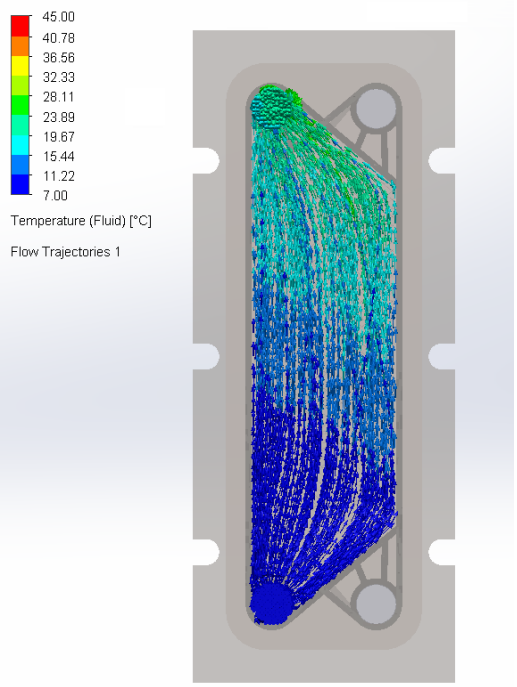

(a) Chilled Water Flow (bottom to top)

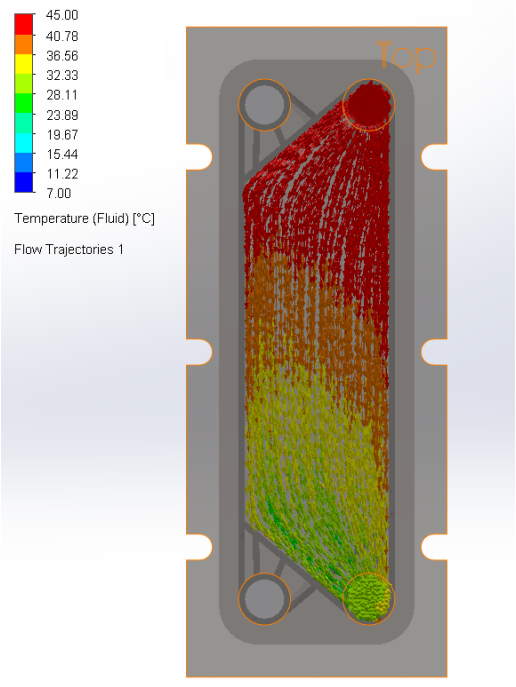

(b) DI Water Flow (top to bottom)

Figure 4.6: Front view of change in T across 40-plate PHE with v=1.25 m/s and $T_{hin} = 45°C$

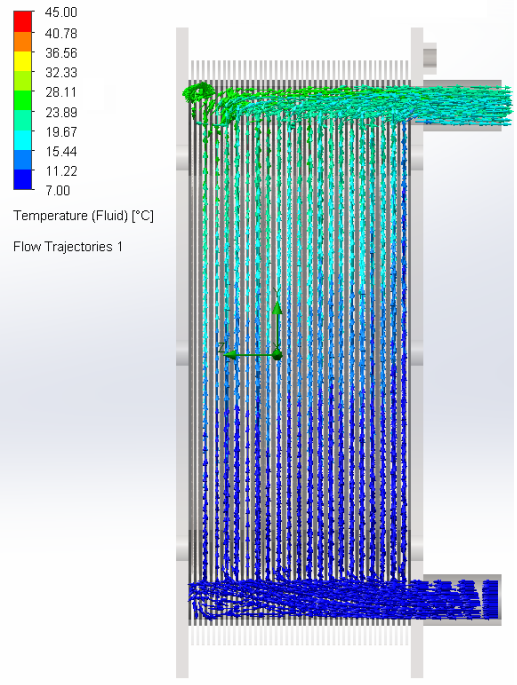

(a) Chilled Water Flow (bottom to top)

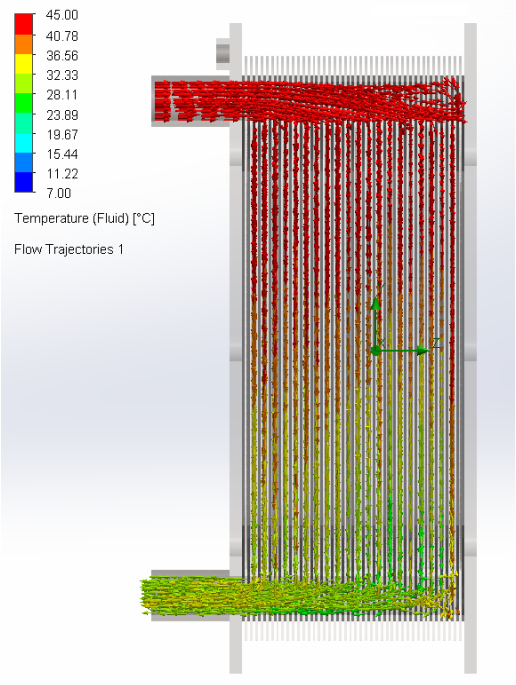

(b) DI Water Flow (top to bottom)

Figure 4.7: Side view of change in T across 40-plate PHE with v=1.25 m/s and $T_{hin} = 45°C$

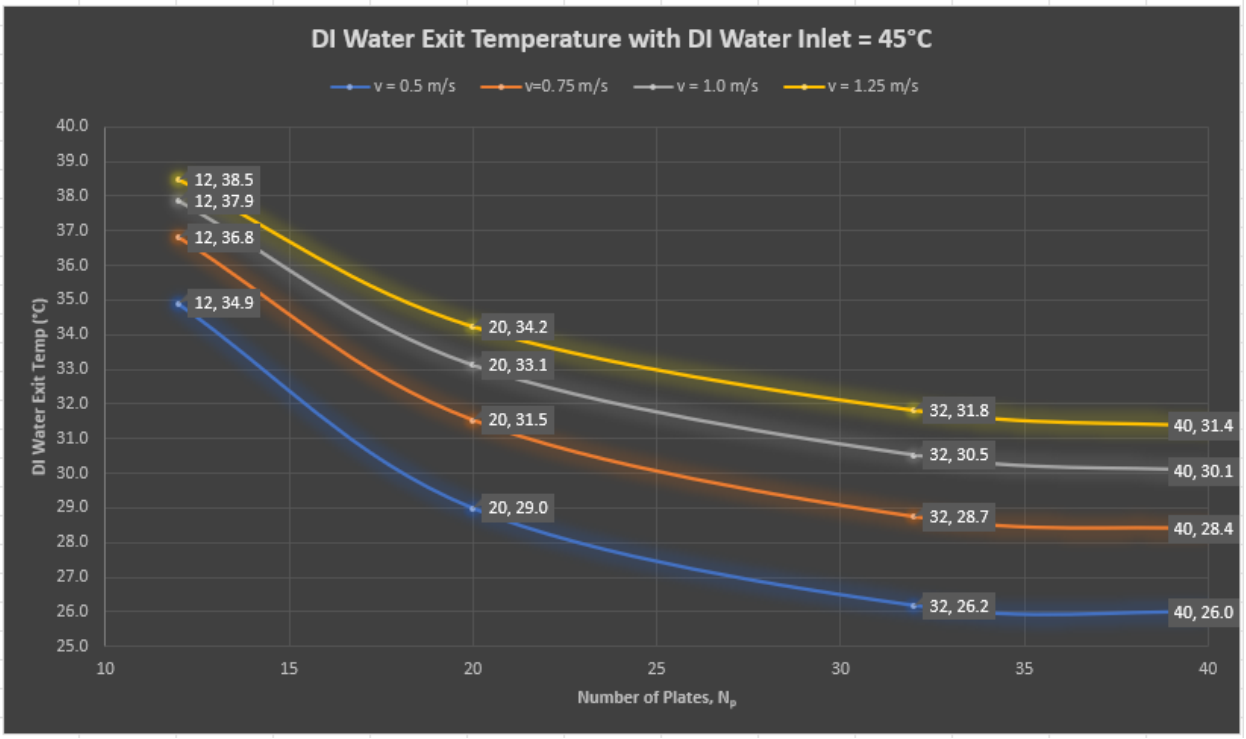

Figure 4.8: T_{DIout} across various PHE plate stacks and velocities with $T_{hin} = 45°C$

4.2.3 Surface Area Analysis

By applying Equation 3.1, it is clear that adjustments to the heat transfer surface area are achieved in distinct increments, each corresponding to the surface area offered by a single plate. Consequently, incorporating more plates into the PHE leads to a proportional enhancement in the heat transfer rate, $\dot{Q}$. This relationship is depicted in Figure 4.9 below, demonstrating how the heat transfer rate increases as as the number of plates increases. Appendix C illustrates similar graphs for T_{DIin}= 35°C and 40°C.

4.2.4 Pressure Analysis

Section 3.1 discusses the impact of the chevron angles on the overall pressure drop across the PHE, noting that larger corrugation angles lead to higher pressure drops, whereas smaller angles tend to reduce them. The plates in the modeled PHE possess a chevron angle of 45°, and analyzing the pressure drop through the PHE is necessary for comprehending its effects on the broader cooling system architecture.

Although MIL-DTL-15730N [29] presents requirements for permissible pressure drops for STHEs onboard surface vessels, pressure drop requirements for PHEs are not explicitly addressed. These standards were nevertheless applied as guidelines for the PHE design, setting a maximum operational pressure drop limit of 6 $\frac{lb_f}{in^2}$ as illustrated in Figure 4.10.

The pressure drop across the PHE is influenced by three main factors: (1) the pressure drop encountered within the core, specifically the plate passages through which fluid flows, (2) the pressure change caused by elevation in a vertically oriented PHE, such as the modeled

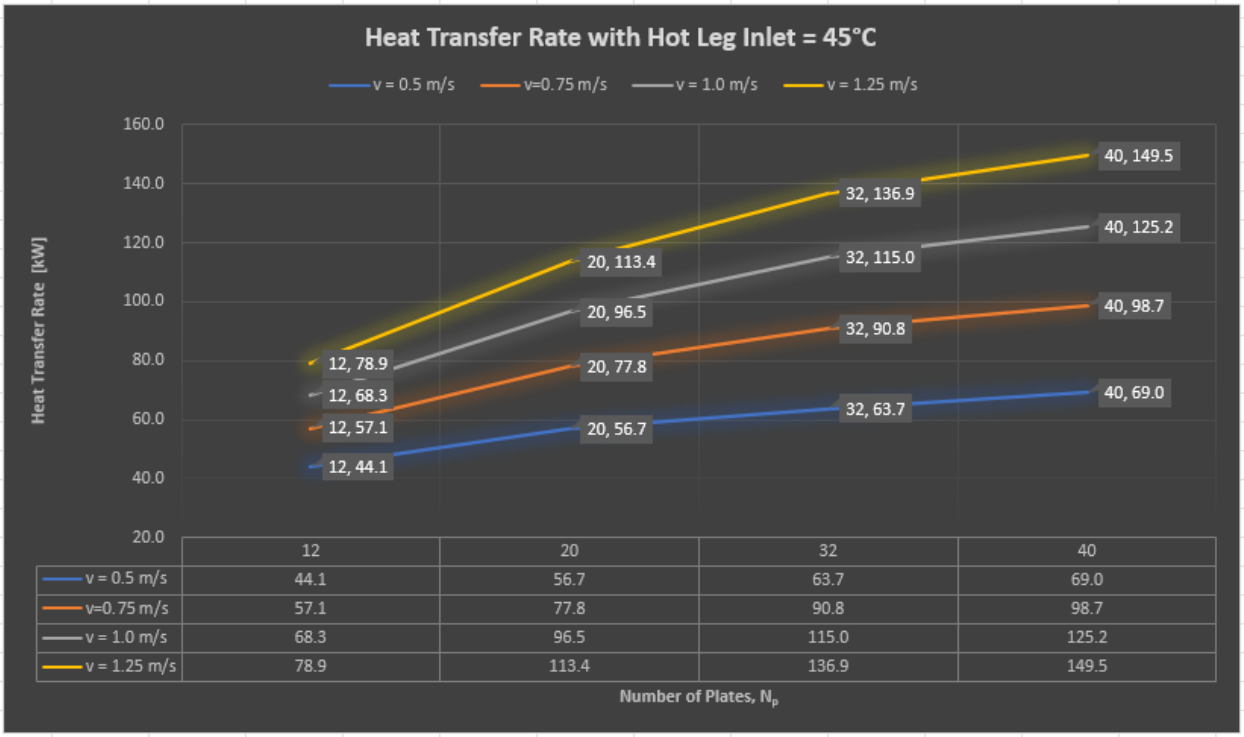

	12	20	32	40
v = 0.5 m/s	44.1	56.7	63.7	69.0
v=0.75 m/s	57.1	77.8	90.8	98.7
v = 1.0 m/s	68.3	96.5	115.0	125.2
v = 1.25 m/s	78.9	113.4	136.9	149.5

Figure 4.9: Heat Transfer Rate versus number of plates at various inlet velocities, with T_{DIin}=45°C

design, and (3) the pressure drop arising from the inlet and outlet nozzles and ports. Shah [21] provides a comprehensive methodology for estimating the pressure drop in a PHE, which has been applied in this context. The analytical calculations presented here aim to reinforce the outcomes observed in the flow simulations by focusing on the pressure drop related to factors (1) and (2). Since boundary conditions for inlet pressures were not incorporated into the flow simulations, factor (3) is excluded from the calculations detailed below.

Thus, the pressure drop across the PHE is given by Equation 4.2:

$$\Delta p = \Delta p_{core} + \Delta p_v \tag{4.2}$$

where

$$\Delta p_{core} = \frac{4fLG^2}{2g_c D_e}\left(\frac{1}{\rho_m}\right) \tag{4.3}$$

and

$$\Delta p_v = \frac{\rho_m g L}{g_c} \tag{4.4}$$

where f is the Fanning friction factor determined in Equation 2.8, L is the plate length (m), G is the fluid mass velocity based on the minimum free area $(\frac{kg}{m^2 s})$, g is the gravitational acceleration factor $(\frac{m}{s^2})$, g_c is the proportionality constant in Newton's second law of motion, D_e is the equivalent diameter of flow passages (m) and ρ_m is the bulk mean fluid density $(\frac{kg}{m^3})$.

TABLE I. Allowable pressure drops.

Cooler type	Fluid side	Allowable pressure drop (lb/in^2)
Main propulsion turbine lubricating oil coolers that use scoop injection of circulating water	Tube (seawater) side	4
	Shell (oil) side	15
Other lubricating oil coolers and freshwater coolers	Coolant side	6
	Cooler fluid side (oil)	12
	Cooled fluid side (freshwater)	6
Hydraulic oil coolers	Tube (coolant) side	6
	Shell (oil) side	25

Figure 4.10: Maximum Allowable Pressure Drop for Surface Coolers [29]

The fluid mass velocity based on the minimum free area is

$$G = \frac{\dot{m}}{A_o} \tag{4.5}$$

where $\dot{m}$ is the mass flow through the core ($\frac{kg}{s}$), and A_o (m^2), the minimum free flow area on one side of the PHE, is

$$A_o = N_p \times b \times W \tag{4.6}$$

where N_p is the number of flow passages, b is the plate spacing (m) and W is the plate width (m). The equivalent diameter of flow passages is equal to twice the plate spacing, $D_e = 2b$ [21].

It is important to recognize that the pressure drop across the PHE will vary slightly between the hot and cold fluids, a discrepancy attributed to differences in density. Table 4.2 outlines the applicable parameters and their associated values in Equations 4.2 through 4.6.

The analytical calculations reveal a modest pressure drop across the PHE, a result that aligns with expectations given the PHE's dimensions. This observation is further supported by the simulation data, which consistently demonstrates a similar trend of minimal pressure variation. The corroborative evidence from these simulations is graphically represented in Figure 4.11 below, illustrating the congruence between theoretical calculations and empirical data in terms of pressure behavior within the PHE.

4.3 Response Surface

The preceding analyses elucidated the impact of variations in inlet velocity, the inlet temperature of DI water, and the number of plates on the heat transfer rate, denoted as $\dot{Q}$. By revisiting Fourier's Equation (as expressed in Equation 4.1), it was established that v_{in} influences the overall heat transfer coefficient (U), T_{DIin} affects the LMTD (ΔT), and the N_p

Parameter	Symbol	Value	Units
Fanning Friction Factor	f	0.188	N/A
Plate Length	L	0.450	m
Plate Width	W	0.150	m
Plate Spacing	b	$2x10^{-3}$	m
Chilled Water Fluid Mass Velocity	G_{cw}	158.3	$\frac{kg}{m^2 s}$
DI Water Fluid Mass Velocity	G_{DI}	156.7	$\frac{kg}{m^2 s}$
Gravitational Acceleration Factor	g	9.81	m/s^2
Gravitational Proportionality Constant	g_c	1	N/A
Equivalent Diameter of Flow Passages	D_e	$4x10^{-3}$	m
Number of Flow Passages	N_p	40	N/A
Minimum Free Flow Area	A_o	0.012	m^2
Chill Water Pressure Drop	Δp	0.794	$\frac{lb_f}{in^2}$
DI Water Pressure Drop	Δp	0.786	$\frac{lb_f}{in^2}$

Table 4.2: Analytical Calculation of Modeled PHE Pressure Drop

directly impacts the heat transfer surface area (A). Nonetheless, there is a keen interest in understanding the collective effect of altering each of these parameters on the heat transfer rate, or more specifically, how a PHE may be optimized for a particular compartment.

Reflecting on the initial discussion of this chapter, it is recognized that the power requirements will vary across different compartments on the ship, leading to diverse cooling demands. Acknowledging these variable cooling demands implies that the heat transfer rate will also fluctuate. For any specific compartment, a target heat transfer rate ($\dot{Q}$) can be defined, thereby serving as an independent variable. In a similar vein, setting a targeted temperature differential across the cold plates ($\Delta T_{ColdPlate}$) enables the LMTD to be specified as another independent variable (because the cold plate temperature differential dictates T_{DIin}, thus establishing the LMTD). Additionally, the inlet fluid velocity can be set as an independent variable. By utilizing the data from the flow simulations (detailed in Appendix B) and establishing $\dot{Q}$, the LMTD, and v_{in} as independent variables specific to a given compartment, the optimal number of plates can be determined.

Using the above approach implies that the quantity of plates in the PHE is a function of these independent variables, allowing for a PHE to be specifically tailored to the compartment's unique requirements and allows Equation 4.7 to be established.

$$N_p = \frac{\dot{Q}}{v_{in}\Delta T} \tag{4.7}$$

where N_p is the number of plates within the PHE, $\dot{Q}$ is the desired heat transfer rate based on shipboard location, v_{in} is the inlet velocity of both the chilled and DI water, and ΔT is the LMTD.

The raw data from Appendix B was input into the mathematical computation program Mathematica and a best fit model of the form defined in Equation 4.7 was applied. The result is given by Equation 4.8 below.

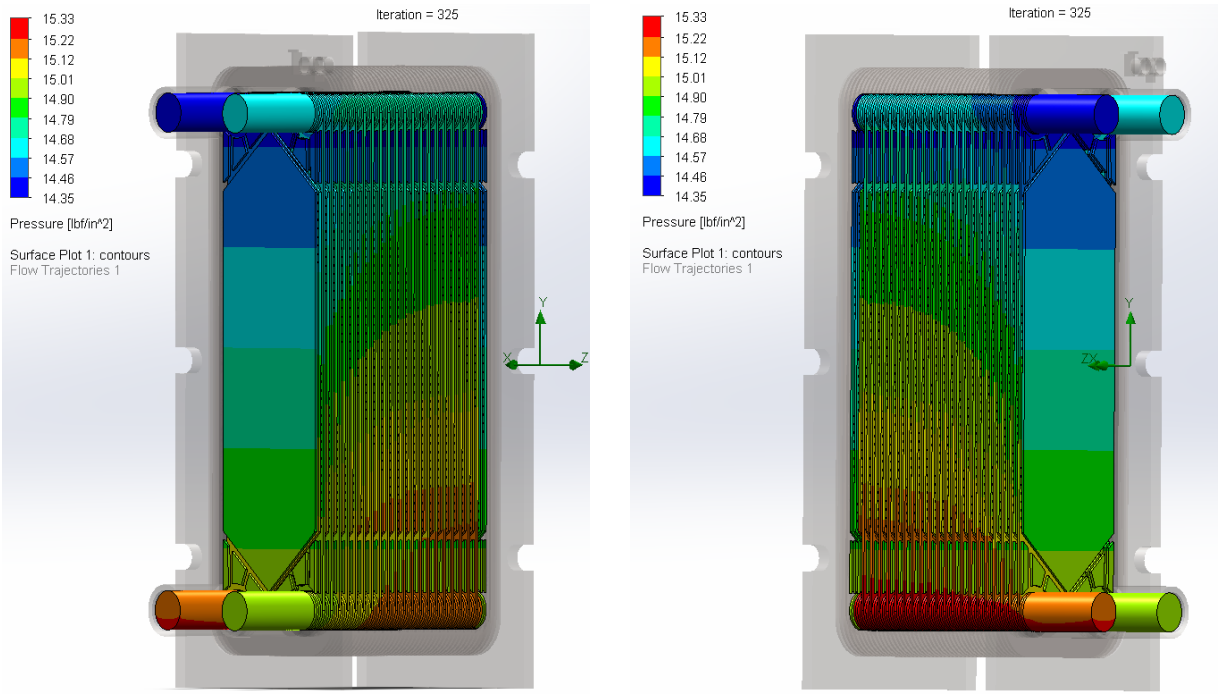

Figure 4.11: Δp across 40-plate PHE with v_{in}=1.25 m/s and $T_{hin} = 45°\text{C}$

$$N_p = \frac{6.20346 \times \dot{Q}}{LMTD \times v_{in}} - 1.41867 \tag{4.8}$$

Equation 4.8 intuitively is of a form similar to Fourier's heat transfer equation given in 4.1. The coefficient of determination (colloquially referred to as the R^2 value) quantifies the extent of the correlation between the linear model and the dependent variables, expressed as a percentage ranging from 0 to 100%. The R^2 value for Equation 4.8 is 0.9632, indicating an excellent correlation.

Utilizing Equation 4.8, a grid of data points was constructed over the specified ranges of $\dot{Q}$, LMTD, and v_{in} in Mathematica. To facilitate smoother plotting, interpolated values for each of these independent variables were generated. Contour surfaces representing discrete increments of the number of PHE plates (N_p) were then plotted across the ranges of $\dot{Q}$, LMTD, and v_{in}. Each discrete value of N_p was distinctly color-coded for ease of visulaization. Figures 4.12 and 4.13 below illustrate this correlation as a 3D plot, generated in Mathematica.

Figures 4.12 and 4.13 demonstrate the customizability of a PHE for specific shipboard compartments. By first identifying the electrical requirements of a compartment, and consequently its cooling needs, the PHE can be customized to meet these precise specifications. This method highlights a dedication to flexibility and adaptability in the design process, allowing for the development of a cooling solution that is not only efficient and effective but also sufficiently versatile to accommodate future technological advancements and evolving requirements.

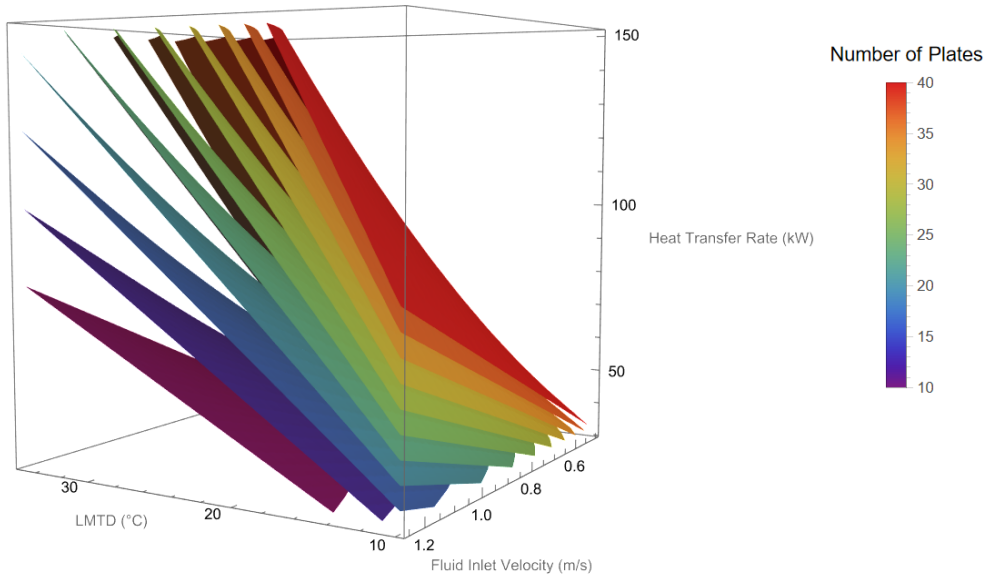

Figure 4.12: View One: Response Model utilizing Equation 4.8, demonstrating N_p as a function of $\dot{Q}$, $LMTD$ and v_{in}

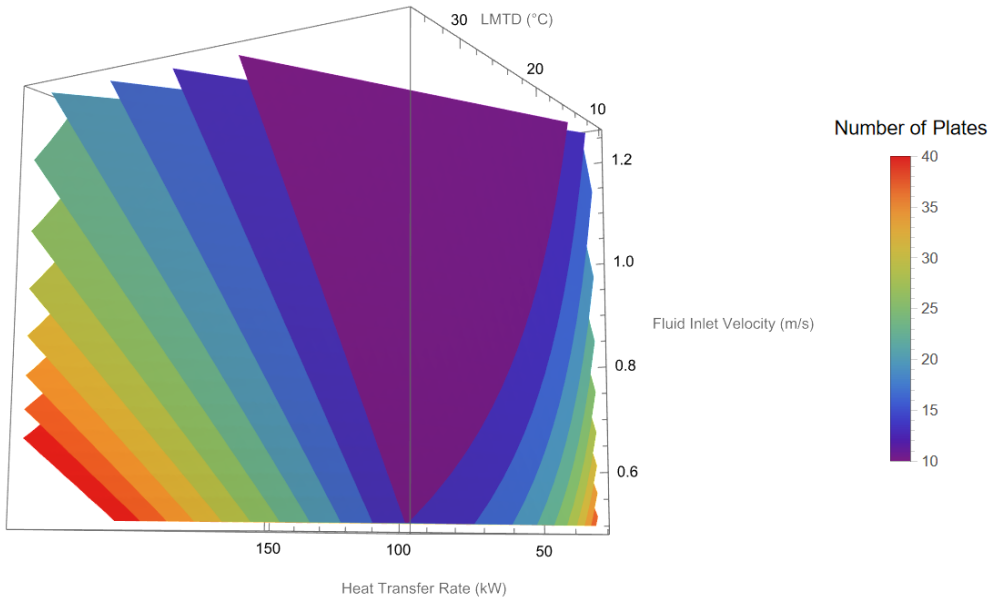

Figure 4.13: View Two: Response Model utilizing Equation 4.8, demonstrating N_p as a function of $\dot{Q}$, $LMTD$ and v_{in}

Chapter 5

Future Work and Conclusion

5.1 Future Work

The findings presented in this thesis offer considerable promise; however, continued investigation is essential to reinforce the Navy's strategies for addressing the thermal management challenges faced by the NiPEC system. While STHEs have been thoroughly studied by Reyes [7] and Chaterjee [11] and show promise, there remains a significant opportunity to explore the potential of utilizing modular plate heat exchangers for implementation into the NiPEC system architecture. The subsequent sections highlight specific research areas that merit further exploration to enhance our understanding and effectiveness in managing these complex thermal systems.

5.1.1 Further Gasket PHE Geometry Exploration

This thesis investigated a plate heat exchanger geometry featuring a single corrugation angle of 45°. Due to the spatial limitations imposed by the PEBB cabinet, as detailed in Section 3.1, the dimensions of the plate, specifically its length and width, must remain relatively constant. However, further exploration into other aspects of plate geometries is warranted.

A pertinent area for future research involves experimenting with varying corrugation angles to assess their impacts on the heat exchanger's performance. One significant aspect to consider is the influence of these angles on the pressure drop across the exchanger. As indicated by Martin [18], higher corrugation angles tend to increase the pressure drop, whereas lower angles may reduce it. Understanding these effects can help in optimizing the design for enhanced efficiency and performance in specific applications.

In addition to experimenting with different corrugation angles for all the plates, the corrugation angles may be varied from plate to plate throughout the PHE. Using different angles of corrugation in the plates within a counterflow plate heat exchanger, compared to using plates all with the same corrugation angle, introduces several significant benefits. Firstly, varied corrugation angles can enhance the heat transfer efficiency of the exchanger. The change in angle can disrupt the flow patterns, leading to increased turbulence within the fluid streams. This turbulence enhances the heat transfer coefficient by promoting more vigorous mixing of the fluid, thus improving the overall heat transfer performance [30].

Secondly, different angles can also reduce the pressure drop across the heat exchanger as previously alluded to. By optimizing the angles of corrugation, the flow can be managed in a way that minimizes resistance, thus reducing the energy required to pump fluids through the exchanger. This can lead to more energy-efficient operations, particularly in systems where the fluid must be moved over long distances or through complex systems.

Moreover, altering the corrugation angles can help in achieving more uniform flow distribution across the plates. Uniform flow distribution prevents areas of low velocity, which are prone to fouling and sedimentation, thereby maintaining the operational efficiency and prolonging the lifespan of the heat exchanger[30]. As demonstrated in Section 4.2.1, maintaining higher velocities throughout the PHE will also enhance the overall heat transfer coefficient.

5.1.2 Fusion-Bonded PHEs

While the benefits of gasketed plate heat exchangers have been explained, exploring fusion welded plate heat exchangers presents an attractive avenue, especially for shipboard applications. Some key advantages and reasons are listed below [31].

- **Enhanced Durability and Reliability** Fusion welded plate heat exchangers, unlike their gasketed counterparts, do not use gaskets between the plates. This eliminates potential weak points where leaks and gasket degradation might occur, making them more durable and reliable, particularly in the harsh environments encountered at sea. This property could significantly reduce maintenance requirements and operational downtime.

- **Increased Operational Pressure and Temperature Ranges** Fusion welded heat exchangers can operate at higher pressures and temperatures compared to gasketed heat exchangers, making them suitable for demanding applications onboard ships. Research into how these heat exchangers perform under extreme conditions could provide insights into their potential for more energy-efficient and robust heat transfer solutions in maritime environments.

- **Improved Corrosion Resistance** The materials and welding techniques used in fusion welded plate heat exchangers can offer superior resistance to corrosion compared to gasketed options. This is particularly beneficial in maritime applications, where exposure to saltwater and corrosive environments is a constant challenge. Investigating the long-term performance of these exchangers in such conditions could lead to more sustainable and longer-lasting heat management solutions on ships.

- **Compactness and Weight Considerations** In shipboard applications, space and weight are critical considerations. Fusion welded heat exchangers can be designed to be more compact and lighter than traditional gasketed units without compromising performance. Future research could explore innovative designs that optimize heat transfer efficiency while minimizing space and weight, crucial for enhancing the operational efficiency of ships.

- **Potential for Enhanced Heat Transfer Efficiencies** While gasketed plate heat exchangers are already efficient, the structural advantages of fusion welded units, such

as reduced risk of fouling and scaling due to the absence of gaskets, might allow for even higher efficiencies. Research could focus on optimizing plate design and flow configurations to maximize heat transfer rates and efficiency.

- **Environmental Sustainability** With increasing focus on reducing environmental impact, the robustness and longevity of fusion welded plate heat exchangers could contribute to lower lifecycle emissions and waste. Studies could investigate the environmental benefits of deploying these exchangers compared to traditional systems, considering factors like reduced frequency of replacement due to enhanced durability.

- **Regulatory Compliance and Safety** Fusion welded exchangers offer potential safety improvements, such as reduced risk of leaks of hazardous fluids. Research into these aspects could help in designing systems that better comply with stringent safety and environmental regulations prevalent in maritime operations.

5.2 Conclusion

This thesis presents a comprehensive design for a modular, compact, indirect liquid cooling system specifically engineered for NiPEC applications on future all-electric Navy destroyer warships. Building upon the foundational research of previous studies, this work enhances the cooling system architecture through a robust combination of first-principles thermodynamic analysis, multi-physics-based modeling, and numerical analysis. Employing an indirect liquid cooling strategy, the design integrates a closed-loop, pressurized, and distributed cooling circuit that leverages the warship's existing chilled water system, ensuring seamless integration and operational efficiency.

The detailed design and analysis of this compact heat exchanger contribute significantly to the modular construction of both the NiPEC cooling and electrical systems, enabling concurrent assembly. By extracting and applying response surface models, the investigation clarifies the dynamic interdependencies among various response variables, such as the overall heat transfer coefficient and heat transfer rates. These variables are influenced by changes in inlet velocities, temperatures, and the specific geometry of the heat exchanger.

This multifaceted analysis not only refines the system's efficiency but also ensures it meets stringent military standards and aligns with the modular integration requirements of military naval applications. Each component of the cooling system has been thoroughly examined, with all relevant standards and requirements documented, demonstrating promising results for shipwide implementation. The design facilitates ease of use and maintenance by sailors and technicians, making it an ideal solution for enhancing thermal management in naval environments. Specific recommendations have been provided for addressing identified challenges, further emphasizing the system's readiness for deployment in NiPEC applications.

References

[1] C. Cooke, C. Chryssostomidis, and J. Chalfant, "Modular integrated power corridor," in *Electric Ship Technologies Symposium (ESTS), 2017 IEEE*, IEEE, 2017, pp. 91–95.

[2] S. Markle, *IPES - Harnessing Total Ship Energy & Power*, Published: Sea-Air-Space Exposition, 2018.

[3] L. Petersen, C. Schegan, T. S. Ericsen, *et al.*, "Power Electronic Power Distribution Systems (PEPDS)," *ESRDC Website, www.esrdc.com*, 2022.

[4] PMS 320, "Naval power and energy systems technology development roadmap," *Naval Sea Systems Command*, 2019.

[5] J. del Águila Ferrandis, J. Chalfant, C. M. Cooke, and C. Chryssostomidis, "Design of a Power Corridor Distribution Network," in *2019 IEEE Electric Ship Technologies Symposium (ESTS)*, IEEE, 2019, pp. 284–292.

[6] N. Rajagopal, R. Raju, T. Moaz, and C. DiMarino, "Design of a High-Frequency Transformer and 1.7 kV Switching-Cells for an Integrated Power Electronics Building Block (iPEBB)," in *2021 IEEE Electric Ship Technologies Symposium (ESTS)*, Aug. 2021, pp. 1–8. DOI: 10.1109/ESTS49166.2021.9512358.

[7] I. Reyes, "Design and Modeling of the Navy Integrated Power and Energy Corridor Cooling System," M.S. thesis, Massachusetts Institute of Technology, 2022.

[8] C. DiMarino, "Navy Integrated Power Electronics Building Block (iPEBB)," in *Office of Naval Research iPEBB Program Review*, Nov. 2020.

[9] S. Yang, J. Chalfant, J. Ordonez, J. Khan, C. Li, I. Cvetkovic, J. Vargas, M. Chagas, Y. Xu, R. Burgos, *et al.*, "Shipboard PEBB cooling strategies," in *2019 IEEE Electric Ship Technologies Symposium (ESTS)*, IEEE, 2019, pp. 24–31.

[10] J. Padilla, J. Chalfant, C. Chryssostomidis, and C. Cooke, "Preliminary Investigation into Liquid-Cooled PEBBs," in *2021 IEEE Electric Ship Technologies Symposium (ESTS)*, Aug. 2021.

[11] A. Chatterjee, "Design and modeling of shipwide navy integrated power and energy corridor cooling system," M.S. thesis, Massachusetts Institute of Technology, Cambridge, MA, 2023.

[12] Wikipedia, *Plate heat exchanger*, Page Version ID: 1134980654, Jan. 2023. URL: https://en.wikipedia.org/w/index.php?title=Plate_heat_exchanger&oldid=1134980654.

[13] Naval Sea Systems Command, *NSTM Chapter 254 - Condensers, Heat Exchangers and Air Ejectors*, Edition: 3rd, Jan. 2005.

[14] Alfa Laval, *Plate Heat Exchanger*, 2015. URL: https://www.alfalaval.com/contentassets/1a62e93b427c47ec9622df8366237a4d/imageoek7.png.

[15] W. Kays and A. London, *Compact Heat Exchangers*, 3rd. McGraw-Hill, 1984.

[16] Naval Sea Systems Command, *DOD-STD-1399, Section 301: Ship Motion and Attitude*, Published: Department of Defense Interface Standard, Jul. 1986.

[17] D. Underwood and G. Campbell, *Overview of HX Design for USN Power Converters*, 2023.

[18] H. Martin, "A theoretical approach to predict the performance of chevron-type plate heat exchangers," *Chemical Engineering and Processing: Process Intensification*, vol. 35, no. 4, pp. 301–310, Jan. 1996, ISSN: 0255-2701. DOI: 10.1016/0255-2701(95)04129-X.

[19] J. Hesselgreaves, *Compact Heat Exchangers: Selection, Design, and Operation*. Pergamon, 2001.

[20] C. Sarao Jr, "Design and Modeling of a Uniform Pressure Distribution Mechanism for Increased Power Converter Density in the Navy integrated Power and Energy Corridor," M.S. thesis, Massachusetts Institute of Technology, 2024.

[21] R. Shah and D. Sekulic, *Fundamentals of Heat Exchanger Design*. John Wiley & Sons, 2003.

[22] O. P. Arsenyeva, L. L. Tovazhnyansky, P. O. Kapustenko, and G. L. Khavin, "Optimal design of plate-and-frame heat exchangers for efficient heat recovery in process industries," *Energy*, PRES 2010, vol. 36, no. 8, pp. 4588–4598, Aug. 2011, ISSN: 0360-5442. DOI: 10.1016/j.energy.2011.03.022.

[23] J. H. Lienhard IV and J. H. Lienhard V, *A Heat Transfer Textbook*. Cambridge, MA: Phlogiston Press, 2020. URL: https://ahtt.mit.edu/wp-content/uploads/2020/08/AHTTv510.pdf.

[24] M. Kyed and N. Subic, "Computation of Nusselt numbers in plate heat exchangers using CFD with Reynolds-averaged Navier–Stokes equations," preprint, Apr. 2023. DOI: 10.31224/2955. URL: https://engrxiv.org/preprint/view/2955/version/4199 (visited on 03/10/2024).

[25] Varalka, *All About The Corrugations on Heat Transfer Plates*, 2023. URL: https://www.varalka.com/all-about-the-corrugations-on-heat-transfer-plates.

[26] Naval Sea Systems Command, *NSTM Chapter 505 - Piping Systems*, Edition: 4th, 2008.

[27] Industrial Quick Search, *Plate Heat Exchanger Editorial*. URL: https://www.iqsdirectory.com/articles/heat-exchanger/plate-heat-exchangers.html.

[28] E. Curran, "Manufacturability Assessment of the Navy Integrated Power and Energy Corridor (NiPEC)," M.S. thesis, Massachusetts Institute of Technology, May 2024.

[29] *Coolers, Fluid, Naval Shipboard - Hydrocarbon Base Oil and Freshwater Services*, Published: Department of Defense Detail Specification, Jun. 2021.

[30] K. Thulukkanam, *Heat Exchangers: Classification, Selection, and Thermal Design*, 1st ed. Boca Raton: CRC Press, Feb. 2024, ISBN: 978-1-00-335204-4. DOI: 10.1201/9781003352044.

[31] Alfa Laval, *Fusion-bonded plate heat exchangers*, 2023. URL: https://www.alfalaval.us/products/heat-transfer/plate-heat-exchangers/fusion-bonded-plate-heat-exchangers/.

Appendix A

List of Acronyms

AC Alternating Current

CAD Computer Aided Design

CFD Computational Fluid Dynamics

CuNi Copper-Nickel

DC Direct Current

DI deionized

ESRDC Electric Ship Research and Development Consortium

iPEBB integrated Power Electronics Building Block

iPEBBs integrated Power Electronics Building Blocks

IPES Integrated Power and Energy System

kV kiloVolt

LMTD Logarithmic Mean Temperature Difference

MW Megawatts

MOSFETs Metal-Oxide-Semiconductor Field-Effect Transistors

NAVSEA Naval Sea Service Command

NiPEC Navy integrated Power and Energy Corridor

NPES Naval Power and Energy Systems

NPS Nominal Pipe Size

NPSH Net Positive Suction Head

NSTM Naval Ship's Technical Manual

ONR Office of Naval Research

PEBB Power Electronics Building Block

PEPDS Power Electronics Power Distribution System

PHE Plate Heat Exchangers

SiC Silicon-Carbide

SCH Pipe Schedule

STHE shell-and-tube heat exchangers

TDR Technology Development Roadmap

TIM Thermal Interface Material

VADM Vice Admiral

V Volts

Appendix B

Flow Simulation Raw Data

6 plate pattern (12 plates)	Experiment 1	Experiment 2	Experiment 3	Experiment 4	Experiment 5	Experiment 6	Experiment 7	Experiment 8	Experiment 9	Experiment 10	Experiment 11	Experiment 12
Velocity normal to face (Inlet Velocity of CW) [m/s]	0.5	0.5	0.5	0.75	0.75	0.75	1	1	1	1.25	1.25	1.25
Velocity normal to face (Inlet Velocity of HW) [m/s]	0.5	0.5	0.5	0.75	0.75	0.75	1	1	1	1.25	1.25	1.25
Temperature (Inlet Velocity of HW) [°C]	35	40	45	35	40	45	35	40	45	35	40	45
GG Average Total Pressure [lbf/in^2]	14.79	14.78	14.78	14.89	14.88	14.88	15.03	15.02	15.02	15.20	15.20	15.20
GG Average Heat Transfer Coefficient [W/m^2/K]	1348.43	1353.33	1358.47	1637.07	1644.71	1652.16	1890.33	1899.86	1910.07	2136.58	2150.08	2164.68
SG Average Temperature of HW Exit [°C]	27.72	31.35	34.90	29.14	32.97	36.80	29.94	33.92	37.87	30.42	34.47	38.47
SG Average Temperature of CW Exit [°C]	14.04	15.33	16.61	12.68	13.73	14.80	11.91	12.85	13.80	11.46	12.33	13.24
LMTD [°C]	20.84	24.51	28.14	22.23	26.12	30.00	23.02	27.04	31.03	23.48	27.57	31.61
Qdot [kW]	32.39	38.23	44.07	41.95	49.51	57.13	50.15	59.21	68.33	57.83	68.34	78.88

10 plate pattern (20 plates)	Experiment 1	Experiment 2	Experiment 3	Experiment 4	Experiment 5	Experiment 6	Experiment 7	Experiment 8	Experiment 9	Experiment 10	Experiment 11	Experiment 12
Velocity normal to face (Inlet Velocity of CW) [m/s]	0.5	0.5	0.5	0.75	0.75	0.75	1	1	1	1.25	1.25	1.25
Velocity normal to face (Inlet Velocity of HW) [m/s]	0.5	0.5	0.5	0.75	0.75	0.75	1	1	1	1.25	1.25	1.25
Temperature (Inlet Velocity of HW) [°C]	35	40	45	35	40	45	35	40	45	35	40	45
GG Average Total Pressure [lbf/in^2]	14.75	14.75	14.75	14.81	14.81	14.81	14.90	14.90	14.90	15.02	15.02	15.02
GG Average Heat Transfer Coefficient [W/m^2/K]	1303.70	1310.63	1317.39	1616.04	1623.93	1631.82	1884.99	1894.56	1903.97	2128.71	2139.18	2149.35
SG Average Temperature of HW Exit [°C]	23.46	26.23	28.99	25.29	28.42	31.53	26.45	29.79	33.12	27.26	30.75	34.23
SG Average Temperature of CW Exit [°C]	18.23	20.21	22.20	16.48	18.17	19.86	15.37	16.87	18.37	14.58	15.95	17.31
LMTD [°C]	16.61	19.51	22.39	18.41	21.62	24.83	19.54	22.96	26.37	20.34	23.90	27.46
Qdot [kW]	41.61	49.12	56.67	57.14	67.46	77.85	70.77	83.58	96.47	83.19	98.23	113.38

16 plate pattern (32 plates)	Experiment 1	Experiment 2	Experiment 3	Experiment 4	Experiment 5	Experiment 6	Experiment 7	Experiment 8	Experiment 9	Experiment 10	Experiment 11	Experiment 12
Velocity normal to face (Inlet Velocity of CW) [m/s]	0.5	0.5	0.5	0.75	0.75	0.75	1	1	1	1.25	1.25	1.25
Velocity normal to face (Inlet Velocity of HW) [m/s]	0.5	0.5	0.5	0.75	0.75	0.75	1	1	1	1.25	1.25	1.25
Temperature (Inlet Velocity of HW) [°C]	35	40	45	35	40	45	35	40	45	35	40	45
GG Average Total Pressure [lbf/in^2]	14.73	14.73	14.73	14.78	14.78	14.78	14.85	14.85	14.85	14.93	14.93	14.93
GG Average Heat Transfer Coefficient [W/m^2/K]	1045.93	1052.70	1057.38	1325.12	1332.54	1338.46	1555.53	1563.47	1570.03	1758.20	1766.94	1774.56
SG Average Temperature of HW Exit [°C]	21.39	23.75	26.17	23.23	25.96	28.74	24.51	27.50	30.52	25.45	28.63	31.82
SG Average Temperature of CW Exit [°C]	20.18	22.52	24.97	18.44	20.46	22.58	17.18	18.99	20.88	16.27	17.92	19.64
LMTD [°C]	14.60	17.11	19.59	16.39	19.25	22.08	17.66	20.75	23.82	18.59	21.85	25.09
Qdot [kW]	46.95	55.37	63.69	66.77	78.84	90.84	84.46	99.74	114.95	100.48	118.69	136.85

20 plate pattern (40 plates)	Experiment 1	Experiment 2	Experiment 3	Experiment 4	Experiment 5	Experiment 6	Experiment 7	Experiment 8	Experiment 9	Experiment 10	Experiment 11	Experiment 12
Velocity normal to face (Inlet Velocity of CW) [m/s]	0.5	0.5	0.5	0.75	0.75	0.75	1	1	1	1.25	1.25	1.25
Velocity normal to face (Inlet Velocity of HW) [m/s]	0.5	0.5	0.5	0.75	0.75	0.75	1	1	1	1.25	1.25	1.25
Temperature (Inlet Velocity of HW) [°C]	35	40	45	35	40	45	35	40	45	35	40	45
GG Average Total Pressure [lbf/in^2]	14.7	14.7	14.7	14.8	14.8	14.8	14.84	14.84	14.84	14.92	14.92	14.92
GG Average Heat Transfer Coefficient [W/m^2/K]	938.1	942.6	947.5	1191.3	1197.5	1202.6	1403.06	1409.76	1415.62	1585.80	1592.77	1599.71
SG Average Temperature of HW Exit [°C]	21.3	23.6	26.0	23.3	25.8	28.4	24.39	27.23	30.06	25.25	28.31	31.36
SG Average Temperature of CW Exit [°C]	21.0	23.5	26.0	19.2	21.5	23.7	17.97	19.99	22.02	17.03	18.88	20.73
LMTD [°C]	14.16	16.55	18.96	16.02	18.66	21.35	17.21	20.12	23.02	18.11	21.22	24.32
Qdot [kW]	51.1	59.9	69.0	73.4	85.9	98.7	92.80	108.98	125.22	110.35	129.85	149.46

Figure B.1: Raw Data from Flow Simulations

Appendix C

Additional Flow Simulation Graphs

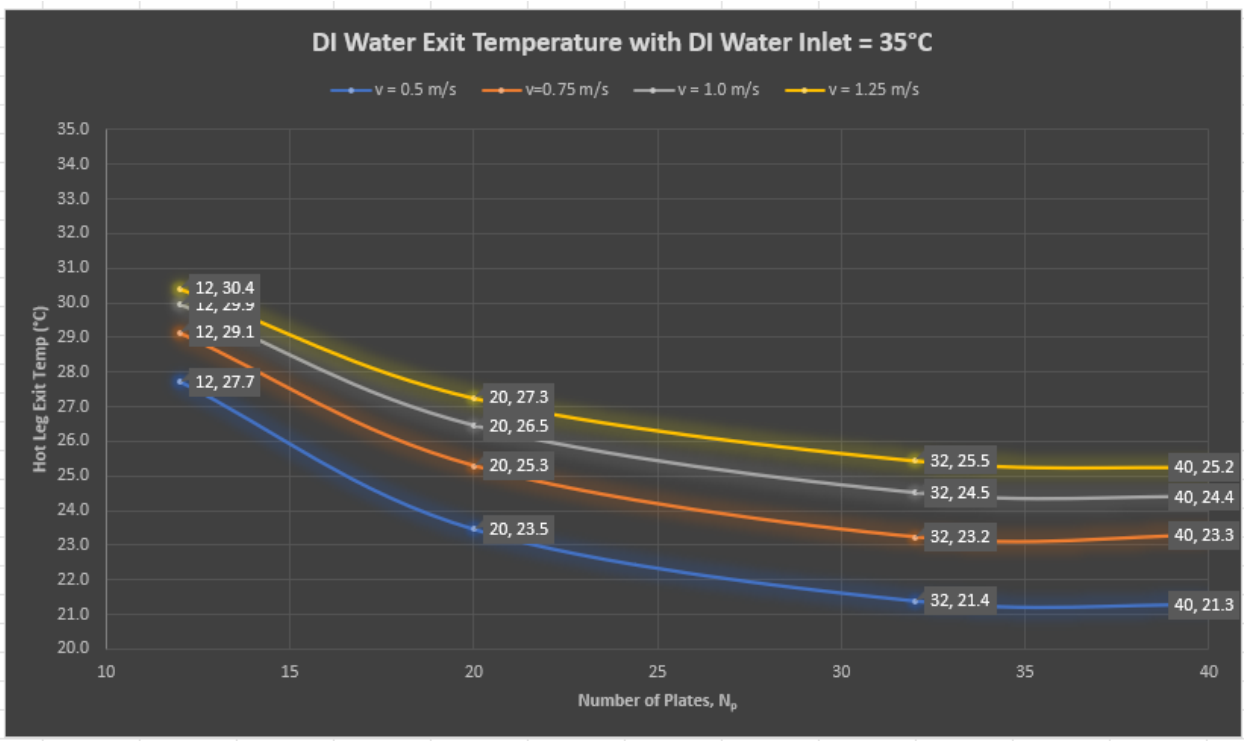

Figure C.1: DI Water Exit Temperature with $T_{DIin} = 35°C$, v=1.25 $\frac{m}{s}$, 40-plates

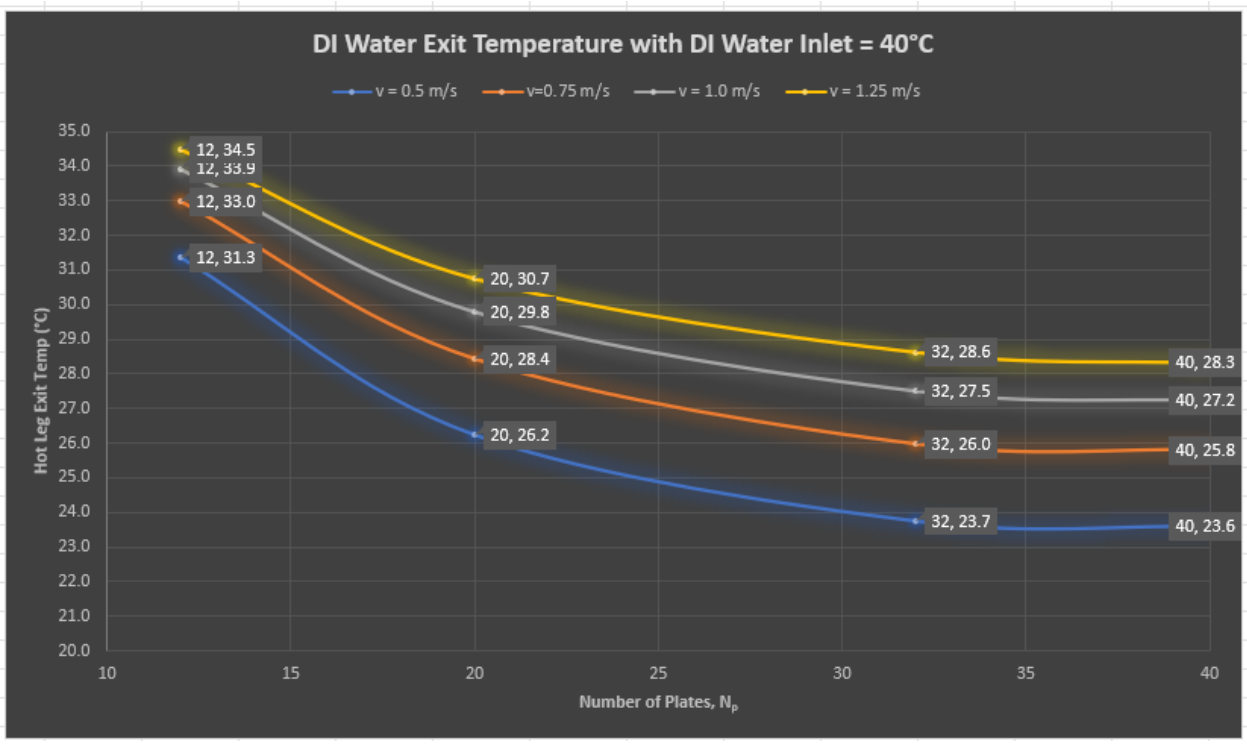

Figure C.2: DI Water Exit Temperature with $T_{DIin} = 40°C$, v=1.25 $\frac{m}{s}$, 40-plate

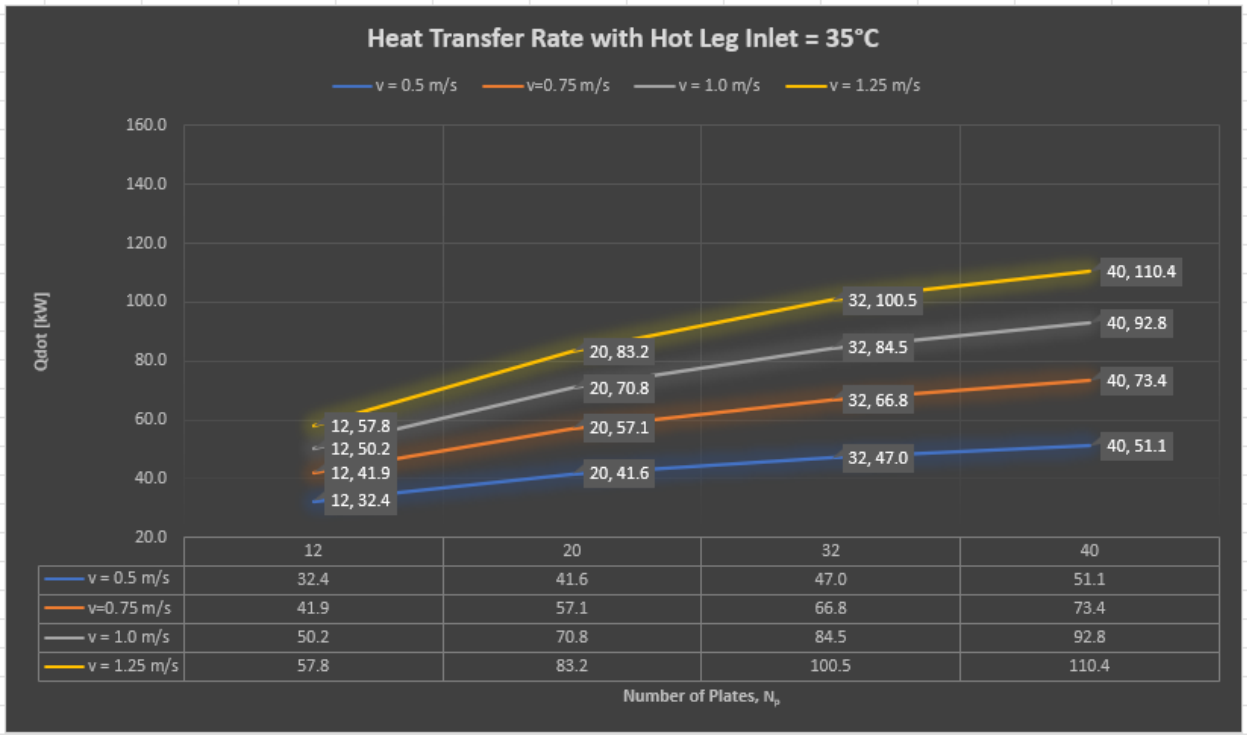

	12	20	32	40
v = 0.5 m/s	32.4	41.6	47.0	51.1
v=0.75 m/s	41.9	57.1	66.8	73.4
v = 1.0 m/s	50.2	70.8	84.5	92.8
v = 1.25 m/s	57.8	83.2	100.5	110.4

Figure C.3: $\dot{Q}$ vs. N_p at various inlet velocities, with T_{DIin}=35°C

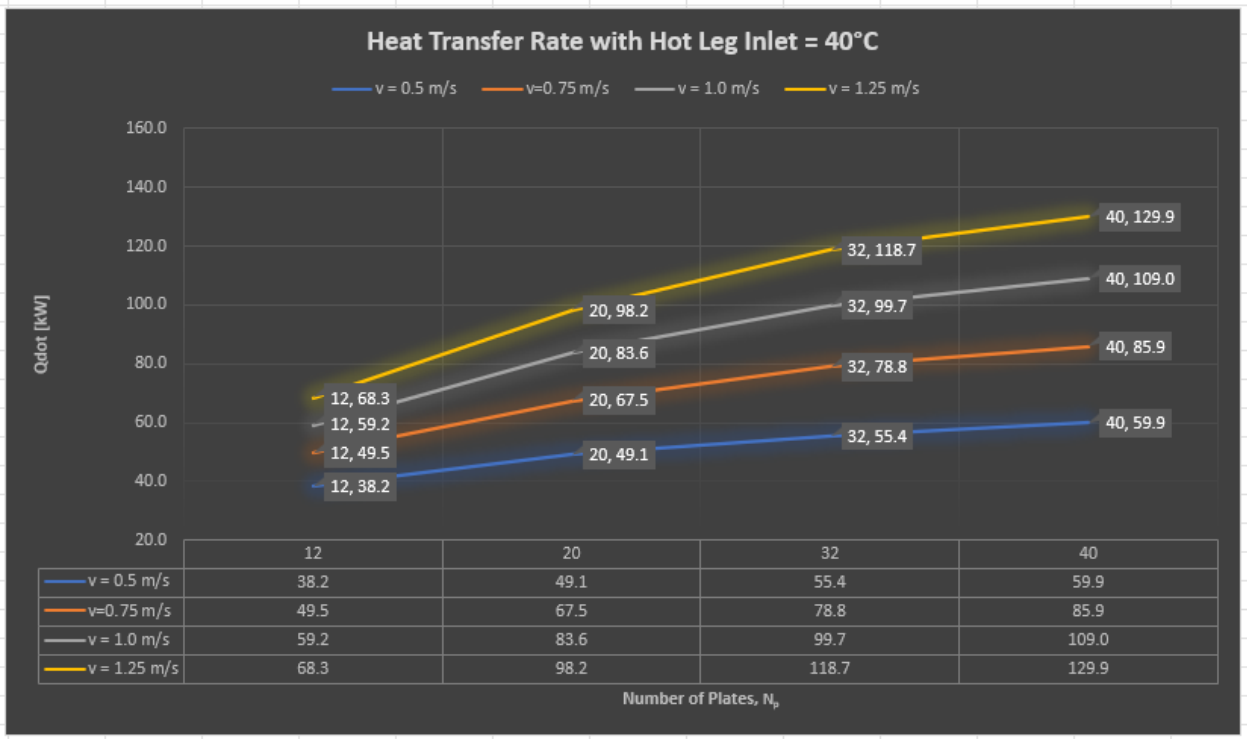

	12	20	32	40
v = 0.5 m/s	38.2	49.1	55.4	59.9
v=0.75 m/s	49.5	67.5	78.8	85.9
v = 1.0 m/s	59.2	83.6	99.7	109.0
v = 1.25 m/s	68.3	98.2	118.7	129.9

Figure C.4: $\dot{Q}$ vs. N_p at various inlet velocities, with T_{DIin}=40°C